Chapter 15
Nanomaterial-Based Antibacterial Paper

Wenbing Hu, Qing Huang, and Chunhai Fan

15.1 Synthesis and Characterization of Nanomaterial-Based Films

The nanomaterial-based film with antibacterial property can be fabricated by physical and chemical methods. Physical methods include spin-coating, dip-coating, vacuum filtration, electrospinning, and magnetron sputtering.

15.1.1 Spin-Coating

Spin-coating is applied to prepare uniform thin film by spreading the solution placed on the flat substrates at a constant rate. The thickness of the film is determined by centrifugal forces controlled by spin speed, solution viscosity, and spin time. TiO_2 film and silver nanoparticles (AgNPs)/TiO_2 composite film have been prepared by spin-coating technology.

TiO_2 nanoparticles have been synthesized using the sol–gel method [2]. In a typical experiment, TiO_2 sol was prepared from the hydrolysis of $Ti(OC_4H_9)_4$: 0.01 mol of $Ti(OC_4H_9)_4$ stirred in ice incubation was mixed with 0.15 mol of ethanol. The ethanol/H_2O/acetylacetone solution (0.1 mol ethanol, 0.02 mol deionized water, 0.01 mol acetylacetone) was added to the $Ti(OC_4H_9)_4$/ethanol solution under stirring in ice incubation, then the mixture was stirred for 2 h. The TiO_2 sol was matured for about 48 h before coating. TiO_2 thin films were coated on titanium plate by the sol–gel spin-coating method with a rotating speed of 2,000 rpm. The resulting films were subjected to heat treatment at 200°C for

W. Hu • Q. Huang (✉) • C. Fan (✉)
Laboratory of Physical Biology, Shanghai Institute of Applied Physics, Chinese Academy of Sciences, Shanghai, China
e-mail: huangqing@sinap.ac.cn; fchh@sinap.ac.cn

N. Cioffi and M. Rai (eds.), *Nano-Antimicrobials*,
DOI 10.1007/978-3-642-24428-5_15,

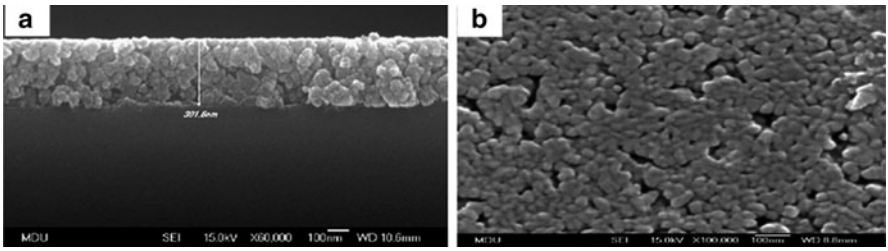

Fig. 15.1 The SEM images of TiO_2 film prepared by spin-coating technology cross-section (**a**) and surface structure (**b**) [3]. Immobilized TiO_2 nanoparticles were ~15.2 ± 0.6 nm

15 min. By repeating this process, TiO_2 thin films with different thicknesses were obtained. Finally, the films were annealed at 500°C for 3 h in air for crystallization. The crystal structure and thickness of TiO_2 film were characterized by scanning electron microscopy (SEM) (Fig. 15.1) [3].

Zhang's [4] and Yang's [5] groups synthesized AgNPs/TiO_2 composite film according to the sol–gel spin-coating method. The SEM images and XRD suggested that the crystallinity and growth of AgNPs were improved by increasing the annealing temperature. Furthermore, the morphology of the AgNPs/TiO_2 composite film could be controlled by simply tuning the molar ratio of the silver nitrate, implying the morphology of composite film became rougher and rougher with the increase in the concentration of silver nitrate, while the diameter of AgNPs decreased. When the molar ratio of Ti^{4+} to Ag^{+} reached 5:1, the composite films were mesoporous. However, the AgNPs attached to the surface of TiO_2 nanoparticles by forming Ag-O-Ti bonds, rather than entering the lattice of the TiO_2 anatase phase [6].

15.1.2 Dip-Coating

The dip-coating method is a simple way to deposit thin film on the substrate. During the process, completely automated by computerized control system, the substrate is slowly dipped into and withdrawn from a tank containing the sol, with a uniform velocity, in order to obtain a uniform film. The film thickness is sensitive to flow conditions in the liquid bath and gas overhead, and is determined by the competition among viscous force, surface tension force and gravity. The faster the substrate was withdrawn, the thicker the film deposited. Many silver nanoparticles (AgNPs)-based films have been fabricated on glass and silica substrates with this procedure [7–10].

Zhang and co-workers [8] have reported a facile two-step method for the preparation of surface-silvered polymer films. The commercial polyimide (PI) film was functionalized by simply dipping the film into dopamine (DOPA) aqueous solution for a period of time. Poly (dopamine) was deposited on the surface of PI

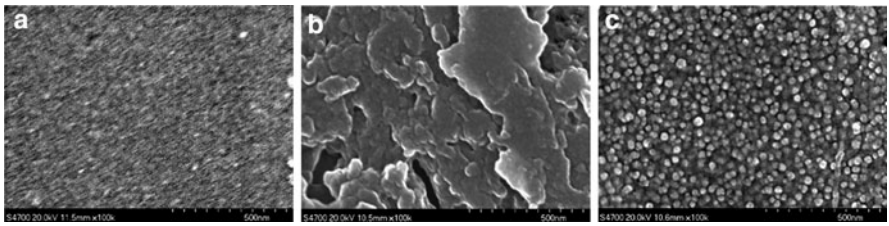

Fig. 15.2 SEM images of (**a**) the pristine PI film, (**b**) the PI-DOPA film, and (**c**) the AgNPs-immobilized PI film [8]

films and formed PI-DOPA films. Then, PI–DOPA films were immersed into an aqueous silver nitrate solution and subjected to UV irradiation in a self-made photochemical reactor for 15 min. The PI-DOPA films deposited with silver were washed thoroughly with doubly distilled water and then dried in a vacuum oven. The distribution and size of the silver nanoparticles could be controlled by changing the reaction time. In the SEM images of films, the surface of PI-DOPA film was much rougher than that of the pristine PI film (Fig. 15.2), resulting from the formation of the distinctive poly (dopamine) layer on the PI film, which facilitated the interlocking with the reduced silver nanoparticles. The silver nanoparticles with the diameter of ~20 nm were uniformly distributed on the surface of PI-DOPA film (Fig. 15.2).

15.1.3 Vacuum Filtration

Graphene oxide (GO) and reduced graphene oxide (rGO) papers were prepared by filtration of the suspension [11]. GO colloidal suspension was prepared from graphite by the modified Hummers method [12]. The GO was reduced to rGO with the aid of hydrazine hydrate [13]. The suspension was filtrated through a PVDF filter membrane (47 mm in diameter, 220 nm pore size) by vacuum at room temperature. The paper could be easily peeled off from the filter paper. The thickness of the paper was controlled by adjusting the volume of the colloidal suspension.

The thickness of GO sheets was ~1.1 nm as measured by atomic force microscope (AFM), suggesting the formation of a single-layer 2-D nanomaterial (Fig. 15.3a), while the thickness of rGO reduced to ~1.0 nm (Fig. 15.3b). The size of GO and rGO varied from nanometers to micrometers. The resulting GO paper was of ~1.5 μm thickness, and the rGO paper was ~4.6 μm as characterized by scanning electron microscope (SEM). Interestingly, the GO paper looked lackluster while the rGO paper was lustrous (Fig. 15.3c, d).

The carbon nanotubes-deposited film or filter were fabricated by vacuum filtration, as described by the Elimelech group [14]. In a typical experiment, multi-walled carbon nanotubes (MWNTs) suspension with the concentration of 0.5 mg/mL in the

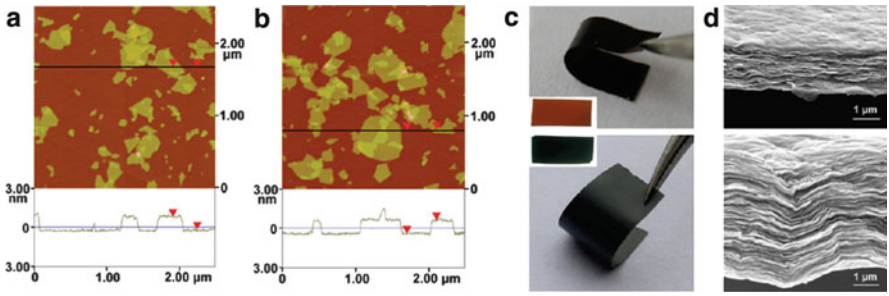

Fig. 15.3 Characterization of GO and rGO nanosheets and paper [11]. (**a**, **b**) AFM images of (**a**) GO and (**b**) rGO sheets. (**c**) Photographs of free-standing and flexible GO (*upper*) and rGO paper (*lower*) (*inset* of (**c**), the photos of GO (*upper*) and rGO (*lower*) paper penetrated by white light). (**d**) The thickness of GO (*upper*) and rGO (*lower*) paper as measured by SEM

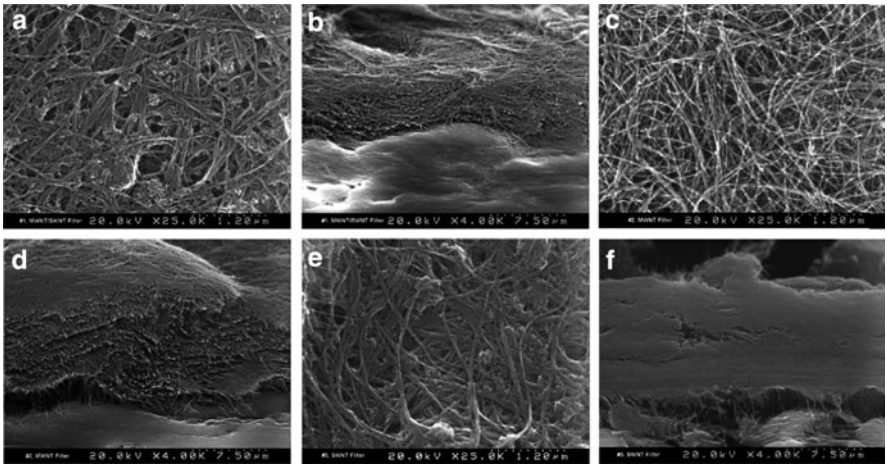

Fig. 15.4 FE-SEM images of the CNTs filters [14]. Aerial views of MWNT-SWNT filter (**a**), MWNT filter (**c**), and SWNT filter (**e**). The cross-section view of MWNT-SWNT filter (**b**), MWNT filter (**d**), and SWNT filter (**f**)

dimethyl sulfoxide (DMSO) was sonicated for 15 min at a power output of 50 W to achieve a more uniform dispersion. Bath sonication of the MWNTs suspension was also performed for 10 s immediately prior to filter deposition to disrupt any aggregates. Deposition of MWNTs from a 5-mL solution was achieved by vacuum filtration through the PTFE membrane (5 μm pore size; Omnipore filters) to attain a loading of 0.27 mg/cm^2 MWNTs on the base filter. The filter was rinsed with 50 mL of ethanol followed by 50 mL of deionized water to remove residual DMSO. And the single-walled carbon nanotubes (SWNTs) filter was made from the suspension with the concentration of 0.1 mg/mL. The MWNTs-SWNTs hybrid filter was made by deposition of SWNTs on the MWNTs filter. As shown in Fig. 15.4, the surface of the MWNTs-SWNTs filter appeared similar to that of the SWNTs filter,

and both filters showed increased bundling of the SWNTs in comparison with the MWNTs filter.

15.1.4 Electrospinning

Schiffman et al. [15] prepared the polysulphone (PSf)/single-walled carbon nanotubes (SWNTs) composite film on the commercial filter by electrospinning technology. In the experimental process, a solution of 4 g PSf and 20 mL DMF was mixed for 24 h. Various amounts of SWNTs (0, 0.4, 20, and 40 mg, corresponding to 0, 0.1, 0.5, and 1.0 wt%, respectively) were added, followed continuous strong ultrasonication for 1 h. The PSf/DMF solution containing SWNTs was loaded into a BD Luer-Lok tip syringe (Becton, Dickinson, Franklin Lakes, NJ, USA). A Precision Glide 21-gauge needle (Becton, Dickinson) was attached to the syringe prior to securing it to an advancement pump (Harvard Apparatus, Plymouth Meeting, PA, USA). Alligator clips were used to connect the positive anode of a high-voltage supply (Gamma High Voltage Research, Ormond Beach, FL, USA) to the needle and the negative anode to a copper plate wrapped in aluminum foil. The speed of the advancement pump, separation distance between the needle and collection plate, and applied voltage were held constant at 0.8 mL/h, 7 cm, and 20 kV, respectively.

The images displayed that PSf mats electrospun with 0, 0.1, 0.5, and 1.0 wt% SWNT loadings appear white, off-white, light ash gray, and deep gray, respectively (Fig. 15.5a), and the TEM images showed that the diameter of electrospun fiber increased with the enhancement of SWNTs contain (Fig. 15.5b–e), owing to incorporation of SWNTs into the electro-spinning solution increasing its conductivity.

15.1.5 Magnetron Sputtering (MS)

Weng's group [16] fabricated AgNPs/polyethylene oxide (PEO) composite film using magnetron sputtering. The fabrication process was accomplished in a bell jar vacuum chamber fed with Ar gas. Before the deposition on the p-silicon (100) wafers, the chamber was initially evacuated to a pressure below 1.3×10^{-3} Pa, refilled with Ar gas three times, and evacuated back to 1.3×10^{-3} Pa. In order to avoid poisoning, the sputtered target was mounted above the substrate, and the gas flowed directly to the pump after diffusing through the substrate. The silver target sputtering with 50 mm diameter, and monomer ethylene glycol dimethyl ether (EGDME) were the sources for AgNPs and PEO polymerization, respectively. DC electric power at 20 W and a suitable working pressure were employed in the MS. For the organic matrix polymerization, EGDME vapor was fed, which kept the constant flow rate by Ar (2 sccm) through the mass flow controller.

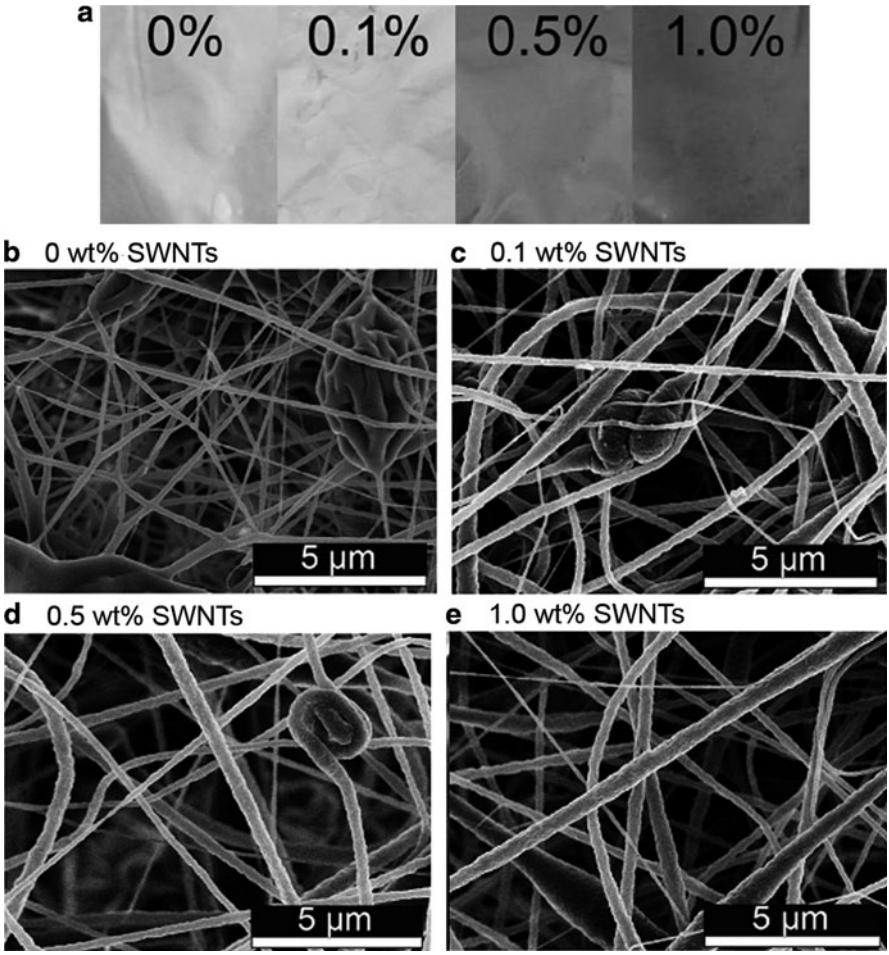

Fig. 15.5 Characterization of PSf/SWNTs films [15]. (**a**) Photographs of PSf films containing 0, 0.1, 0.5, 1.0 wt% loading of SWNTs. (**b**–**e**) The overall fiber SEM images of PSf films containing 0 (**b**), 0.1 (**c**), 0.5 (**d**), 1.0 wt% (**e**) loading of SWNTs

The TEM images and the selected area electron diffraction (SAED) presented the morphology of AgNPs embedded into PEO film. The pattern of discontinuous concentric rings showing in the SAED was characteristic of the silver, suggesting AgNPs in the matrix were of atomic status with preferential crystal orientation. When the working pressure was 0.2 Pa, the diameter of AgNPs with spherical shape was varied ranging from 5 to 10 nm (Fig. 15.6b), while the AgNPs were more than 20 nm when the working pressure was increased to 2.0 Pa (Fig. 15.6a), and the AgNPs shapes appeared spherical, triangular and elliptical, suggesting that the AgNPs diffused on the substrate had aggregated.

The peaks at $2\theta = 38.1°$, 44.2°, 64.4°, and 77.3° that were assigned to {111}, {200}, {220}, and {311} crystalline planes of silver, respectively, also demonstrated

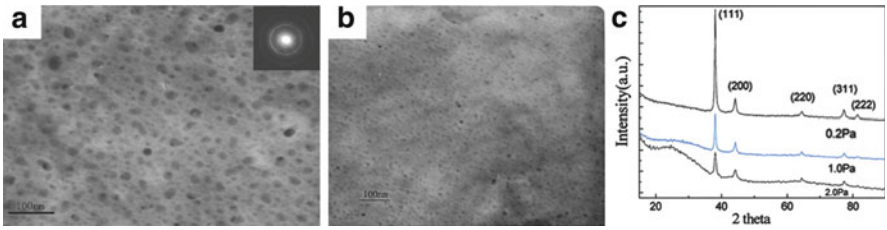

Fig. 15.6 Characterization of AgNPs/polyethylene oxide composite films [16]. (**a**, **b**) TEM images of AgNPs embedded into polyethylene oxide with the working pressure (**a**) 2.0 Pa and (**b**) 0.2 Pa. *Inset* at (**a**) displays the electron diffraction pattern of the AgNPs/polyethylene oxide composite films. (**c**) XRD patterns of AgNPs embedded in AgNPs/polyethylene oxide composite films with different working pressures

that AgNPs in the composite film were still crystal (Fig. 15.6c). Based on this pattern, the size of AgNPs could be calculated using the Scherer Formula $D = K\lambda/\beta\cos\theta$, where K depending on crystallite shape is constant (0.89), λ is the X-ray wavelength, β is the full width at half-max, and θ is the Bragg angle. The sizes of AgNPs were calculated as 7, 11 and 22 nm corresponding to 0.2, 1.0 and 2.0 Pa, respectively, which was in agreement with the TEM results that the AgNPs were grown with the increased working pressure.

15.1.6 Chemical Vapor Deposition

Chemical vapor deposition (CVD), as the most compatible approach to industrial scale production methods, could produce strongly adhesive, robust, durable, and highly active transparent thin films [17]. These film properties contrast with those produced by the coating approach that typically results in thicker films, which are less mechanically robust and often require post-coating annealing. A great many forms of CVD were developed and are frequently referenced in the literature with the different initiating means of chemical reactions and process conditions, such as atmospheric pressure CVD (APCVD), flame-assisted CVD (FACVD), thermal CVD, and so on.

Yates et al. [18] described the deposition of films of titania and copper oxide by atmospheric pressure CVD on pre-coated silica-coated barrier glass substrates. The precursor for TiO_2 film growth was titanium tetraisopropoxide (7.79×10^{-4} mol/min), transported to the reactor by N_2 via a bubbler. The substrate temperature for growth was set to 500°C. The CuO films were grown using an atmospheric pressure flame-assisted CVD coater with a propane/oxygen flame, previously described in detail [19]. The substrate temperature was set at 400°C. An aqueous solution of 0.5 M $Cu(NO_3)_2$ was nebulized into a carrier of N_2, through the flame and onto the substrate. The resulting films were shown to be polycrystalline. The XRD and AFM studies demonstrated that both growth of TiO_2 above and below CuO film was in the form of anatase, and CuO

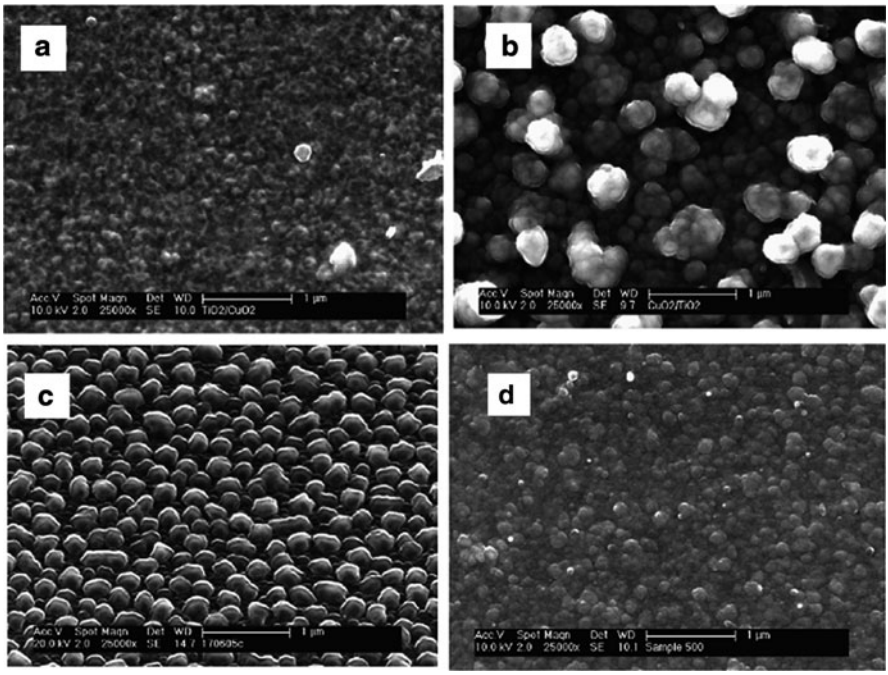

Fig. 15.7 SEM images of (**a**) CuO film over TiO_2, (**b**) TiO_2 film over CuO, (**c**) CuO film and (**d**) TiO_2 on the glass substrates [18]

film deposited above the TiO_2 film was in the form of copper II oxide, and Cu I oxide when CuO film was deposited on the TiO_2 film with over 61 nm thickness. Furthermore, CuO film deposited over TiO_2 film by FACVD consisted of an island growth-type structure of packed spherical nanoparticles, with size of ~100 nm (Fig. 15.7a), which was very similar in appearance to that of a single TiO_2 layer (Fig. 15.7d), rather than that of a single CuO film (Fig. 15.7c), suggesting the CuO film deposition was very much influenced by the underlying structure, in this case the change from amorphous smooth silica to crystalline titania. However, the TiO_2 film over thick CuO film had a much more pronounced particulate structure than the other surfaces, due to the existence of Cu_2O within this TiO_2 film (Fig. 15.7b).

15.2 Antibacterial Activity of Nanomaterial-Based Films

The antibacterial activity of nanomaterial-based films, including metal oxide nanoparticles (e.g., TiO_2 and ZnO), AgNPs, graphene, and carbon nanotubes, were determined against the model bacterium *E. coli*.

15.2.1 TiO_2-Based Film

TiO_2 nanoparticles were in the forms of anatase, brookite and rutile [20], where anatase TiO_2 was the most studied semiconductor after the discovery of its photocatalytic behavior [21]. So far, much attention has been focus on the photocatalysis and photo-induced hydrophilic effect mechanisms, improvement of photocatalytic activity by advancement of the microstructure, and applications including antimicrobial, and self-cleaning behaviors [22]. The biocidal activity of TiO_2 was first demonstrated by Matsunaga and co-workers [23]. Subsequently, a great deal of the considerable literature has shown that TiO_2 nanoparticles can kill cancer cells, bacteria, viruses, and algae under UV illumination [24–28], resulting in important applications in the disinfection of air, water, and surfaces. But most of these early work involved TiO_2 suspension and planktonic organisms. Recently, researchers had focused on the biocidal activity of the thin films of TiO_2 deposited on the substrate surfaces [29–32].

15.2.1.1 Comparison of the Test Methods

In order to compare the antibacterial activity of TiO_2 film prepared from different approaches, Yates' group [33] firstly compared the two-test methods, BS ISO 27447:2009 and in house standard (BS EN 13697). In a typical experiment, bacterial cells were collected by centrifugation at 12,000 rpm for 5 min, and washed three times with physiological saline solution. The cells were resuspended in a 1:500 dilution of Nutrient Broth and adjusted to OD 0.1 ~ 0.2 at 600 nm in a spectrophotometer to give approximately 2×10^8 colony-forming units (CFU) per milliliter. In the BS ISO 27447:2009 method, 50 μL of cells suspension was inoculated onto each 20-mm^2 test sample and covered with a square of 1-mm^2 borosilicate glass to ensure close contact between the culture and the film. The samples were placed in 50-mm-diameter Petri dishes containing moistened filter paper to prevent drying out of the suspensions. The samples were irradiated with Blacklight Blue lamps with a maximum UV light intensity of 0.26 mW/cm^2. Plain borosilicate glass was used for a control experiment. Samples were removed after incubation time and immersed in 20 mL of sterile physiological saline solution, following vortexed for 60 s to resuspend the bacteria. The viability count was performed by serial dilution and plating on nutrient agar in triplicate and incubation at 37°C for 48 h. However, in the house standard method, the cells were resuspended in sterile water, and the samples were not covered with glass, but incubated in 55-mm-diameter Petri dishes kept humid by adding 2 mL sterile water under UVA lamp irradiation of 2.24 mW/cm^2. They found the control experiment remained viable after 24 h irradiation with only a 1-log reduction, while there was a 2-log reduction in the house standard method after 6 h irradiation. This difference could be attributed to the low concentration of Nutrient Broth in the resuspension medium in the BS ISO 27447:2009 method which meant that the bacterial cells

were less stressed and remained viable for longer. Also, the number of the viable cells in the BS ISO 27447:2009 method was much larger that of the viable cells in the house standard method, owing to the reduced illumination levels by approximately tenfold, and the existence of oxidizable material in the resuspension medium (1/500 dilution of Nutrient Broth rather than distilled water) competing with the bacteria for reactive oxygen species (ROS).

15.2.1.2 Antibacterial Activity of TiO_2 Films

Kikuchi et al. [34] found that the survival ratio of *Escherichia coli* on the TiO_2 film under black light illumination (1.0 mW/cm^2) decreased to a negligible level within 1 h (Fig. 15.8a), while the UV light only caused ~50% sterilization within 4 h. And the TiO_2 film in the dark did not affect the survival ratio, indicating that the film itself was not toxic for *E. coli*, which was also demonstrated by Sunada et al. [29]: when the initial cell concentration was 2×10^5 CFU/mL (Fig. 15.8b), bacterial cells on the TiO_2 film was killed within only ~90 min under the UV light illumination (1.0 mW/cm^2). And they emphasized that the survival curve did not follow a simple single exponential decay process with the increasing of illumination time, but appeared to consist of two steps, a very low rate photokilling step, followed by a higher one, which was observed regardless of the initial cell concentration in the range of 2×10^5–2×10^8. In the case of an initial cell concentration of 2×10^5 CFU/mL, the rate constants of the first and second steps were 0.015 and 0.085 min^{-1}, respectively, which was close to those obtained in the powder systems [35, 36]. Further studies

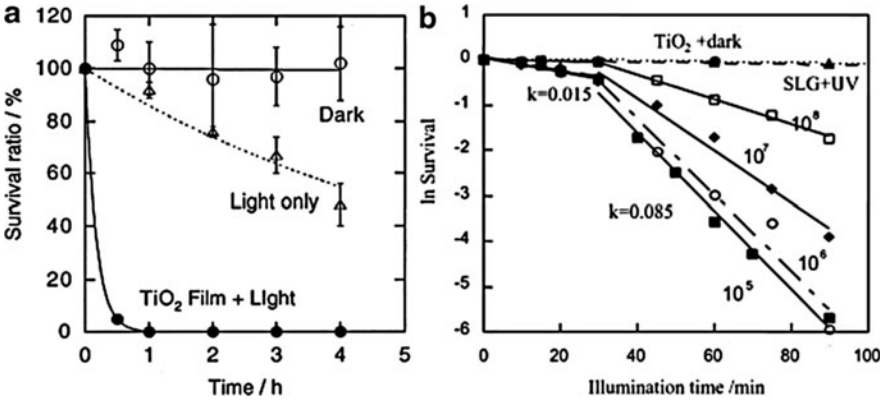

Fig. 15.8 (**a**) Survival ratio of *E. coli* with and without a TiO_2 thin film under black light illumination (1.0 mW/cm^2) and with a TiO_2 thin film in the dark [29]. (**b**) The log plot of the survival of *E. coli* cells versus illumination time. The cell suspension was incubated on TiO_2 film under UV illumination (1.0 mW/cm^2). The initial cell concentrations were 2×10^5 CFU/mL (■), 2×10^6 CFU/mL (○), 2×10^7 CFU/mL (♦), 2×10^8 CFU/mL (□), respectively. Survival was also determined for cells (2×10^5 CFU/ml) on the TiO_2 film in the dark (●), and on normal glass (soda-lime glass, *SLG*) without TiO_2 film under UV illumination (▲) (1.0 mW/cm^2)

showed that various bacteria, *E. coli*, *Staphylococcus aureus*, and *Pseudomonas aeruginosa*, etc., were killed rapidly on TiO_2 film under UV illumination (320–380 nm, 1.0 mW/cm^2) [37].

15.2.1.3 Antibacterial Activity of TiO_2-Based Composite Films

In order to overcome the disadvantages that the antibacterial activity of TiO_2 film was strongly weakened under the dark conditions and very low UV intensity, TiO_2 film deposited with the selected metal (and metal oxide) nanoparticles has been developed, such as silver and copper, which presented intrinsic antibacterial activity.

Zhang et al. [38] found AgNP-doped TiO_2 film exhibited much stronger antibacterial abilities toward both Gram-negative *E. coli* and Gram-positive *S. aureus* than that of pure anatase TiO_2 nanoparticles films. When the films were illuminated under 365 nm UV light (0.1 mW/cm^2), almost all the bacteria were killed by AgNP-doped TiO_2 films (>99.9%), while the antimicrobial value only reached 77.0% and 72.9% for *E. coli* and *S. aureus* on pure anatase TiO_2 nanoparticle film, respectively. More importantly, the antimicrobial activities of the AgNP-doped TiO_2 film were still maintained even without exposure to UV light, such that the sterilizing rate reached 99.1% and 99.4% to *E. coli* and *S. aureus*, respectively. These results indicated that AgNPs promoted the antibacterial activity of TiO_2. Mai et al. [4] also synthesized AgNP-doped TiO_2 film on titanium plates by the sol–gel process. They found AgNPs deposited on TiO_2 film were of metallic nature and could grow to larger ones with an increase in the annealed temperature (Fig. 15.9a–c), and that the smaller the size of AgNPs, the better was the antibacterial ability whether in the dark or under visible light (Fig. 15.9d, e).

Sunada et al. [30] prepared the copper-deposited TiO_2 film, and demonstrated that the resulting film could inhibit the growth of copper-resistant *E. coli* not under dark conditions, but with a very weak UV intensity of 1 μW/cm^2, which corresponds to the typical UV intensity of indoor light (Fig. 15.10a). However, the copper-deposited TiO_2 film could represent photocatalytic antibacterial activity toward the normal *E. coli* (Fig. 15.10b). Foster et al. [33] also found CuO-doped TiO_2 film and CuO-TiO_2 co-deposited film gave a 2-log reduction after 4 h in the dark, and when the incubation time increased, the antibacterial activity of CuO-doped TiO_2 film was higher than that of CuO-TiO_2 co-deposited film, resulting from the reduced availability of CuO surface on the co-deposited film. However, under the UV illumination, the antibacterial activity of both CuO-doped TiO_2 and co-deposited film was greatly enhanced, giving a >6-log reduction after 2 h. Furthermore, Ondok et al. [39] and Sato et al. [40] reported that the antibacterial ability of CuO-doped TiO_2 film was enhanced when either the content of Cu or the UV intensity increased.

Recently, Dai et al. [31] reported photocatalytic hydrogen generation using a TiO_2 nanoparticle/MWNTs nanocomposite under visible light irradiation, which suggests that the photocatalytic activity of the MWNTs-doped TiO_2 nanoparticle

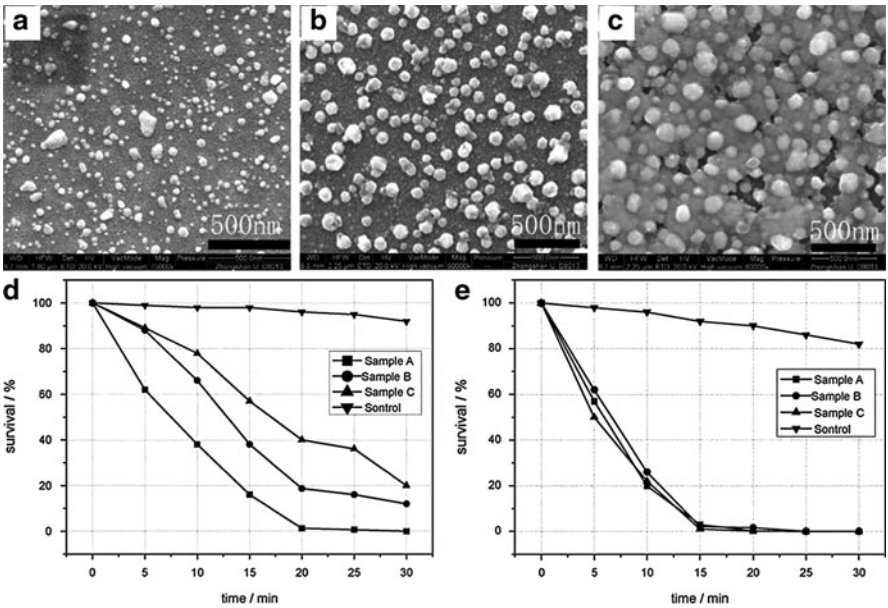

Fig. 15.9 (**a**–**c**) SEM images of the AgNPs-doped TiO_2 films annealed at different temperature. The sizes of AgNPs in the films were 20 ~ 30 nm (**a**), 60 ~ 80 nm (**b**) and >100 nm (**c**). (**d**, **e**) Survival curves of *E. coli* for the films (**d**) in the dark and (**e**) at visible light irradiation. The smaller size of AgNPs have the better antibacterial ability whether in the dark or under visible light [4]

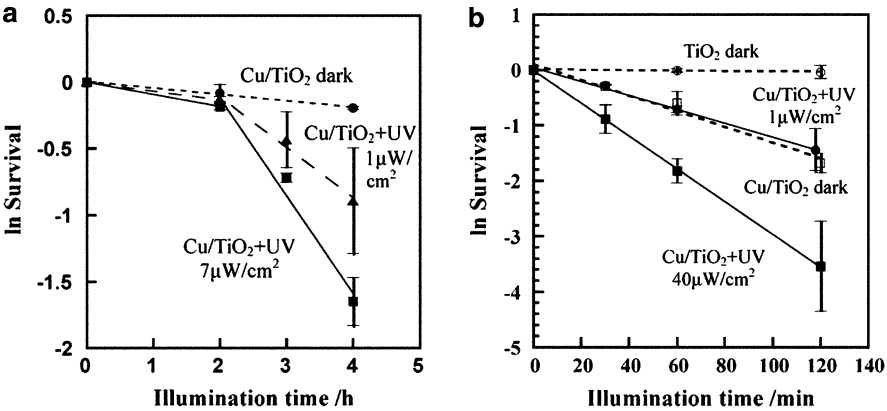

Fig. 15.10 (**a**) Changes in the survival of normal *E. coli* cells under the different illumination intensity. Cells (2×10^5 CFU/mL) were incubated on the TiO_2 film (O) and on the copper-deposited TiO_2 film (□) under dark conditions, respectively. The suspension was also incubated on the copper-deposited TiO_2 film under UV illumination at a UV light intensity of 40 μW/cm^2 (■) and 1 μW/cm^2 (●). (**b**) Changes in survival of copper-resistant *E. coli* cells on the copper-deposited TiO_2 film under dark condition (●) and under UV illumination at light intensity of 7 μW/cm^2 (■) and 1 μW/cm^2 (▲) [30]

was excited by visible light irradiation, rather than UV irradiation. Akhavan et al. [41] and Oh et al. [42] have shown that the MWNTs/TiO_2 nanocomposite could inactivate bacteria under the visible light irradiation and in the dark. Further, Akhavan et al. [32] tested the antibacterial property of MWNTs-doped TiO_2 film by varying the content of MWNTs and the post-annealing temperature. They found that the antibacterial activity of the MWNT-doped TiO_2 films in the dark gradually increased by increasing the MWNTs content of the films, independent from the post-annealing temperature (Fig. 15.18a). Especially, when the MWNTs contain reached 20 wt%, the MWNTs-doped TiO_2 films annealed at 450°C showing an ability of complete inactivation of the bacteria under the visible light irradiation for 1 h, while the corresponding film annealed at 100°C could kill 93% of the bacteria under the same conditions.

15.2.1.4 Durability and Regenerate Ability of TiO_2 Films

Book and co-workers [43] demonstrated the durability and regenerate ability of TiO_2 film prepared by CVD. TiO_2 films were repeatedly cycled through the biocidal test procedure followed with a cleaning process (film was sonicated in methanol and then chloroform for 30 min), and then characterized the film photoactivity by the stearic acid test. They found no measurable reduction in maintained photoactivity, within the accuracy of the test, over three test cycles (Fig. 15.11b).

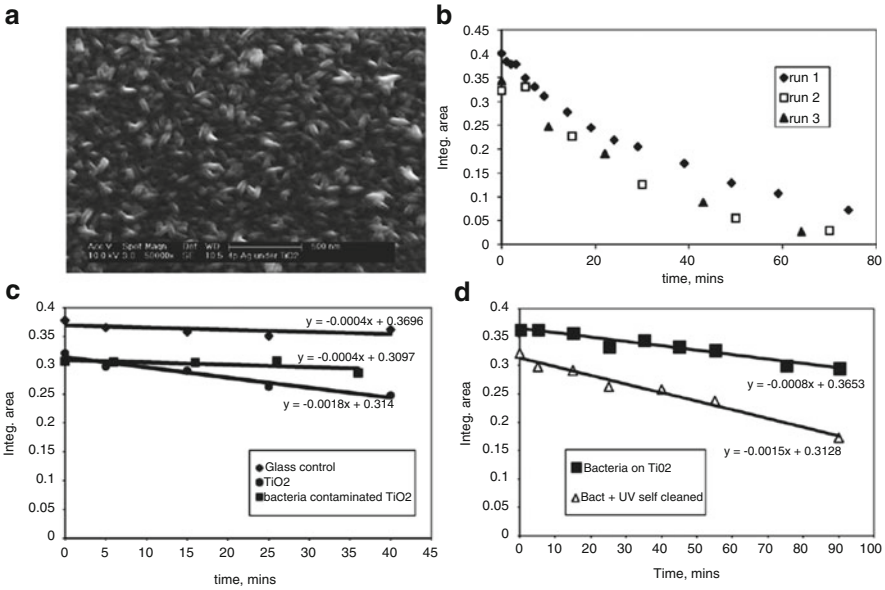

Fig. 15.11 (**a**) SEM image of TiO_2 over AgNPs films. (**b**) An example sample showing the retention of photoactivity after bioactivity testing. (**c**) Photoactivity after bio-contamination and (**d**) photoactivity after UV "self-regeneration" [43]

Additionally, it was known that TiO_2 film was mechanically durable, owing to the TiO_2 was hard and scratch resistant and had the longest term stability.

The TiO_2 surface can decompose organic contamination with the aid of UV light, suggesting the application of TiO_2 photocatalysis to novel "self-cleaning" techniques, which was first demonstrated by Watanabe et al. in 1992 [44]. And water could penetrate the molecular-level space between the stain and the superhydrophilic TiO_2 surface, so the surface was maintained clean with the supply of water current even though the photons excited by UV light may be insufficient to decompose the adsorbed stain [45]. After the biocidal test procedure, the TiO_2 film was visibly contaminated with dead bacteria residues, leading to significant reduction of photocatalytic activity (Fig. 15.11c). However, after the film contaminated with dead bacteria residues was treated with an additional UV irradiation, the film recovered a significant percentage of the original activity (Fig. 15.11d).

15.2.2 ZnO-Based Films

Owing to low cost, easy availability and unique chemical and physical properties, ZnO nanoparticles has sparked much interest. Jones et al. [46] reported that ZnO nanoparticles presented higher antibacterial activity on *S. aureus* than other metal oxide nanoparticles. Padmawathy et al. [46] demonstrated that nano-ZnO showed enhanced antibacterial activity as compared with bulk ZnO. And Zhang et al. [47] reported that the antibacterial activity of ZnO nanoparticles increased with decreasing particle size, and the dispersants (Polyethylene Glycol and Polyvinylpyrolidone) did not much affect the antibacterial activity of ZnO nanoparticles but enhanced the stability of the suspensions. Thus, Bajpai et al. [48] prepared ZnO/chitosan film, and revealed that the film showed excellent antibacterial action against *E. coli*. And Chandramouleeswaran et al. [48] demonstrated that nano-ZnO/polypropylene film could kill almost all *Staphylococcus aureus* and *Klebsiella pneumoniae* with just nano-ZnO filler at a 3% level of loading. Shalumon et al. [49] demonstrated that sodium alginate/poly(vinyl alcohol)/nano-ZnO composite nanofiber mats could suppress the growth of *Staphylococcus aureus* and *Escherichia coli*.

15.2.3 AgNPs-Based Films

The antimicrobial properties of silver were well known to the ancient Egyptians and Greeks. Since then, silver has been used in different fields in medicine and surface coating for many years [50], due to a strong cytotoxic effect toward a broad range of microorganisms and remarkably low human toxicity compared to other heavy metal ions. Silver nanoparticles (AgNPs) also show efficient antimicrobial properties, because of their extremely large surface area which provides better contact with

microorganisms. Recently, not only silver ions or a silver nanoparticle colloid but also all kinds of silver-based films have attracted more and more attention.

Akhavan et al. [51] synthesized AgNPs film on the SiO_2 thin film, and found that the AgNPs film presented strong antibacterial activities against *E. coli* and *S. aureus* bacteria with relative rates of reduction of the viable bacteria of 1.05 and 0.73 h^{-1} for initial concentration of ~10^5 CFU/mL, respectively, and the difference was attributed to amount of peptidoglycan in the cell wall structure. The antibacterial activity of the AgNPs films was dependent on the AgNPs size corresponding to the surface-to-volume ratio. The smaller AgNPs with larger surface area could lead to a much greater bactericidal effect [52].

However, AgNPs were not stable and readily aggregated, and AgNP oxidation was accelerated by illumination with white lamps in air [53], resulting in the reduction of antibacterial activity. Therefore, the AgNP-based composite films, such as AgNP/TiO2 film [54], AgNP/chitosan film [55–57], AgNP/polyethylene oxide film [16], AgNP/hyaluronan/poly (dimethyldiallylammonium chloride) film [58], AgNP/sodium alginate film [59], AgNP/polyvinyl alcohol [60], AgNP/polyester film [61], AgNP/poly (ethylenimine) film [7], AgNP/polyvinyl sulphonate film [62], AgNP/poly (vinyl alcohol)/ploy (L-lactic acid) film [63], and AgNP/N-(2-aminoethyl)-3-aminopropyl-trimethoxysilane (DIAMO) film [64] were considered to overcome those challenges. Akhavan et al. [65] found the antibacterial activity of TiO_2-capped silver nanorods film in the dark was stronger than that of TiO_2-capped AgNPs film, with 2.34 h^{-1} for the relative rate of reduction of the number of viable bacteria. Vimala et al. [66] successfully fabricated the AgNP/chitosan film by a three-step process: silver ion-poly (ethylene glycol) matrix preparation, addition of chitosan matrix, and removal of poly (ethylene glycol) from the film matrix. The AgNP/chitosan film can inhibit the growth of *E. coli*, *Bacillus*, and *K. pneumoniae*, and especially, after 350 min of incubation, AgNPschitosan film can killed ~75% of *E. coli*.

15.2.4 CNTs-Based Films

Carbon nanotubes are pseudo-one-dimensional carbon allotropes of high aspect ratio, high surface area, and excellent material properties, such as ultimate electrical and thermal conductivities and mechanical strength, which offer a wide range of opportunities and application potential in biology and also antibacterial nonmaterial [67]. Narayan et al. [68] showed that nanotube films formed via high temperature laser ablation of graphite on silicon completely inhibited bacterial colony formation. However, the nanotube structure was not well controlled and the process may not be amenable to many biomedical materials. Kang et al. [69], Rodrigues et al. [70] and Brady-Estévez et al. [71] tested the antibacterial activity of SWNTs filter against *E. coli*, showing inactivation of ~80% of *E. coli* after only 20 min incubation (Fig. 15.12) [71]. And then Kang et al. [69, 72] has revealed that the SWNTs filter presented higher antimicrobial activity than a MWNTs-coated filter, and the

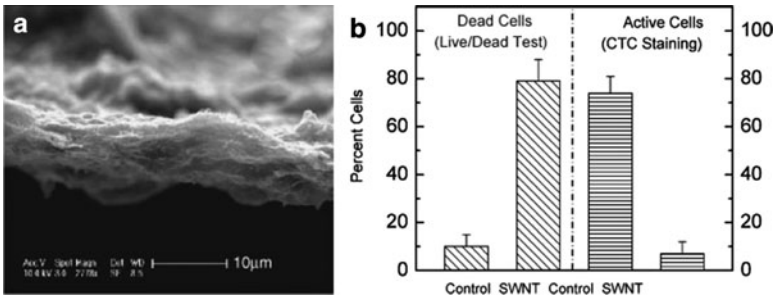

Fig. 15.12 (**a**) SEM image of the cross-section of a layer of SWNTs filtrated onto the PVDF membrane. The SWNTs film displayed highly porous structures. (**b**) Inactivation (*left row*) and metabolic activity (*right row*) of *E. coli* cells retained on the SWNTs film and on the control PVDF membrane. Inactivation test results based on the Live/Dead test showing the percent of *E. coli* cells that were not viable. Metabolic activity results based on CTC staining indicated the percent of metabolically active *E. coli* cells [71]

SWNT-coated filter could inactivate >60% of microorganisms in river water and wastewater treatment plant samples, while natural organic matter did not influence its antimicrobial activity [72]. Brady-Estévez et al. [14] prepared a novel SWNTsMWNTs hybrid filter which was composed of a thin SWNTs layer on top of a thicker MWNTs layer supported by the PTFE membrane, and found that the hybrid filter not only exhibited high log removal of several model viruses (MS2, PRD1, T4) by depth filtration but also provided high levels of inactivation of model bacteria (*E. coli* K12 and *Staphylococcus epidermidis*), as well as microbes from river water and treated wastewater effluent.

They found the physicochemical properties (e.g., diameter, length, aspect ratio, sample purity, structural defects) determined the antimicrobial activity of MWNTs-coated filter, and functionalized [sonication in a mixture of H_2SO_4 and HNO_3 (3:1 v/v) for 1 h] and short MWNTs-coated filters represented excellent antibacterial activity, possibly due to increased density of the open tube ends [73]. However, Yang et al. [74] considered that longer SWNTs filters exhibited stronger antibacterial activity. Vecitis et al. [75] demonstrated for the first time that SWNTs electronic structure was a key factor regulating SWNTs antibacterial activity, and found that antibacterial activity of the high percent metallic (>95%) SWNTs filter was higher than that of the low percent metallic (<5%) SWNTs one, owing to the high percent metallic SWNTs-induced oxidative stress after SWNTs–bacteria contact and physical perturbation of the cell membrane.

In order to improve the antibacterial property of CNTs filter, large amounts of CNTs-based composite filters were introduced. Simmons et al. [76] prepared a flexible composite film by depositing SWNTs coated with polyvinylpyrrolidone-iodine (PVPI) in water, and found that the PVPI-coated SWNTs film could slowly release antiseptic iodine, resulting in the effective antibacterial property over 48 h incubation. Aslan et al. [77] found that *E. coli* and *S. epidermidis* viability and metabolic activity were significantly diminished on the SWNTs/polymer poly(lactic-co-glycolic acid)

(PLGA) film, and were correlated with SWNTs length and concentration (<2 wt%). Schiffman et al. [15] observed that the loss of viability of *E. coli* on the electrospun polysulphone/SWNTs mats was directly correlated to increased SWNTs incorporation within the mat, ranging from 18% for 0.1 wt% SWNTs to 76% for 1.0 wt% SWNTs, and the antimicrobial action of the polysulphone/SWNTs mats occurred after a short contact time of 15 min or less. Pangule et al. [78] incorporated conjugates of MWNTs with lysostaphin (Fig. 15.13a), a cell wall degrading enzyme, into films to impart bactericidal properties against methicillin-resistant *S. aureus* (MRSA) and *S. epidermidis*, and found that these enzyme–MWNTs films were highly efficient in killing MRSA (>99% within 2 h) without release of the enzyme into solution (Fig. 15.13b), and these films were reusable and stable under dry storage conditions for a month (Fig. 15.13c). Zhou and Qi [79] synthesized a novel epilson–polylysine–MWNTs nanocomposite by covalent attachment of epilson-polylysine on MWNTs with hexamethylene diisocyanate as the coupling agent,

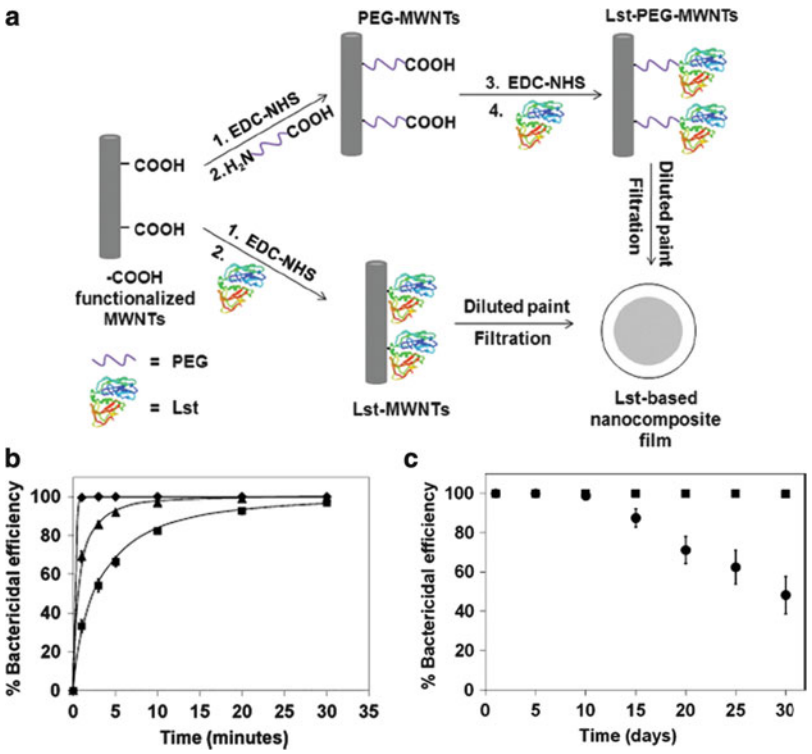

Fig. 15.13 (**a**) Scheme of antimicrobial nanocomposite films containing lysostaphin-MWNTs. (**b**) Comparison of bactericidal effect of Lst-MWNTs film (■) and Lst-PEG-MWNT film (▲) with the native enzyme (♦). These enzyme-MWNTs films were highly efficient in killing MRSA without release of the enzyme into solution. (**c**) Operational (●) and storage stability (■) of films containing 4% w/w Lst in the form of Lst-PEG-MWNT. The films were stored in dry conditions and at room temperature in between the two use cycles [78]

and found that the epilson–polylysine–MWNTs film showed improved antibacterial activities and excellent anti-adhesive efficacy against *P. aeruginosa* and *S. aureus*.

Additionally, owing to outstanding electron transmitting property of CNTs, the antibacterial activity of CNTs films was enhanced by the aid of applied potential. Vecitis et al. [80] prepared an electrochemical MWNTs microfilter by depositing MWNTs on the PTFE membrane, and demonstrated that the MWNTs filter was effective for complete removal of bacteria by sieving and multilog removal of viruses by depth filtration in the absence of electrolysis, while concomitant electrolysis during filtration resulted in significantly increased inactivation of influent bacteria and viruses; especially, application of 2 and 3 V for 30-s post-filtration inactivated >75% of the sieved bacteria and >99.6% of the adsorbed viruses, leading to the number of bacteria and viruses in the effluent reaching below the limit of detection.

15.2.5 Graphene-Based Films

Graphene consisted of a monolayer of carbon atoms which were tightly packed into a two-dimensional crystal. Since the seminal work of Geim and coworkers on free-standing graphene in 2004 [81], many potential applications of graphene were actively pursued owing to its outstanding mechanical stiffness and electronic transport property [82, 83], such as nano-electronic devices [84], sensors [85], solar cells [86], and nanocomposite materials [82].

Hu et al. [11] demonstrated that the two water-dispersible graphene derivatives, graphene oxide (GO) and reduced graphene oxide (rGO) nanosheets, could effectively suppress the growth of *E. coli* cells, and the free-standing GO and rGO papers also presented antibacterial activity. And Akhavan et al. [87] further demonstrated that GO and rGO nanowalls could kill Gram-positive *S. aureus* bacteria. Park et al. [88] fabricated the Tween/rGO paper by simple filtration of a homogeneous aqueous colloidal suspension of a Tween/rGO hybrid, and found that the tween/rGO paper could inhibit nonspecific binding of Gram-positive bacteria *Bacillus cereus*, while rGO paper without tween showed nonspecific bacteria binding (Fig. 15.14).

15.3 Mechanism of Nanomaterial-Based Films Antibacterial Activity

15.3.1 TiO_2-Based Films

As we know, the antibacterial activity of TiO_2 film was attributed to its photocatalysis property. In order to reveal the important molecules directly interacting with bacterial cells, Kikichi et al. [34] designed the membrane-separated

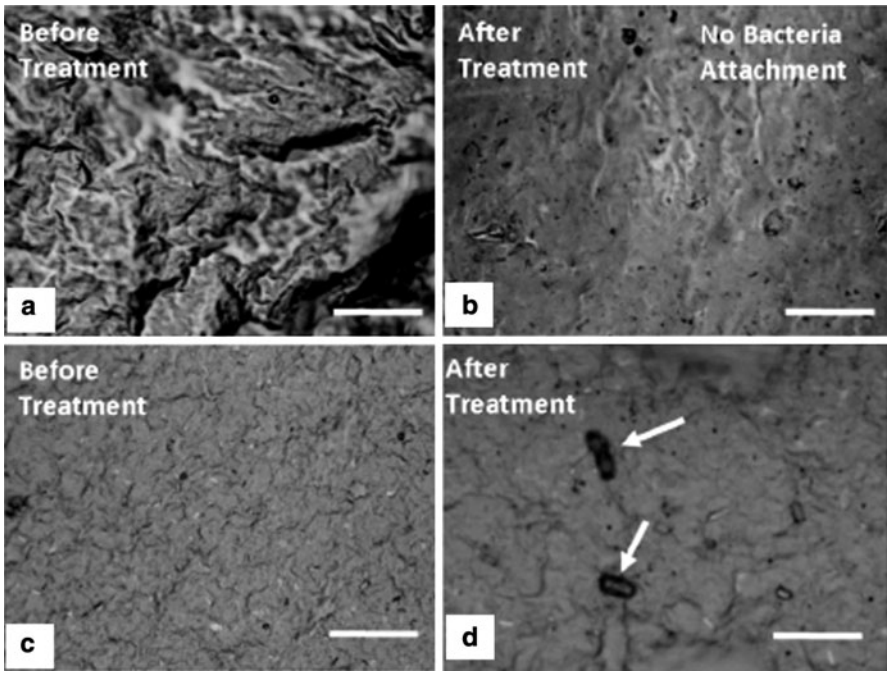

Fig. 15.14 (**a**, **b**) Optical microscopy image of the tween/rGO paper before and after the treatment with a DI-water suspension of the mature *Bacillus* cereus cells. The tween/rGO paper shows no bacterial attachment. (**c**, **d**) Optical microscopy image of the rGO paper before and after the bacterial treatment. The rGO paper shows bacterial attachment (marked by *arrows*) [88]. All scale bars 10 μm

system to fence out TiO_2 film and *E. coli* suspension by the PTFE membrane (50 μm thickness, 0.4 μm pore size). They found the survival ratio of bacteria on the film surface improved with the increase in both mannitol concentration and pH value which could suppress the activity of radical molecules ($^{\bullet}OH$ and $^{\bullet}O_2^-$), and that the existence of catalase in the suspension could enhance the bacterial survival ratio, suggesting the formation of radical molecules and H_2O_2 in the suspension under the UV illumination. So, it was clear that various reactive species (e.g., $^{\bullet}OH$, $HO_2^{\bullet}$, H_2O_2) were produced by UV illumination of TiO_2 in the presence of water and air by the following reactions [89, 90]

$$TiO_2 + h\nu \rightarrow e^- + h^+ \tag{15.1}$$

<Reduction reaction>

$$\begin{aligned} &O_2 + e^- \rightarrow O_2^- \\ &O_2^- + H^+ \rightarrow HO_2^{\bullet} \\ &HO_2^{\bullet} + HO_2^{\bullet} \rightarrow H_2O_2 + O_2 \\ &H_2O_2 + e^- \rightarrow OH^- + {}^{\bullet}OH \end{aligned} \tag{15.2}$$

<Oxidation reaction>

$$H_2O + h^+ \rightarrow {}^{\bullet}OH + H^+$$
$${}^{\bullet}OH + {}^{\bullet}OH \rightarrow H_2O_2$$
$$H_2O_2 + 2h^+ \rightarrow 2H^+ + O_2 \quad (15.3)$$

These reactive oxygen species (ROS) can decompose organic compounds and extinguish cellular activity.

Sunada et al. [29] studied the photokilling process of *E. coli* on the TiO_2 film by means of AFM, which suggested that bacterial cells decomposed from the outside of the cell, resulting from the TiO_2 film photocatalysis (Fig. 15.15a–c). Additionally, Kühn et al. [91] observed that the killing rates of bacteria were dependent on the thickness and structure of cell walls. Based on these observations, they found that the photokilling of bacteria on the illuminated TiO_2 surface could be divided into three stages (Fig. 15.15d). First, disordering of the outer membrane of bacterial cells by reactive species ($^{\bullet}OH$, $^{\bullet}O_2^-$, H_2O_2). The outer membranes of *E. coli* cells were decomposed partially by the reactive species produced by the TiO_2 photocatalyst, while the bacteria cell viability was not lost very efficiently. Second, disordering of the inner membrane (the cytoplasmic membrane) and killing of the cell. Owing to the change of the permeability to reactive species when the partial outer membrane was decomposed, reactive species easily reached and attacked the inner membrane,

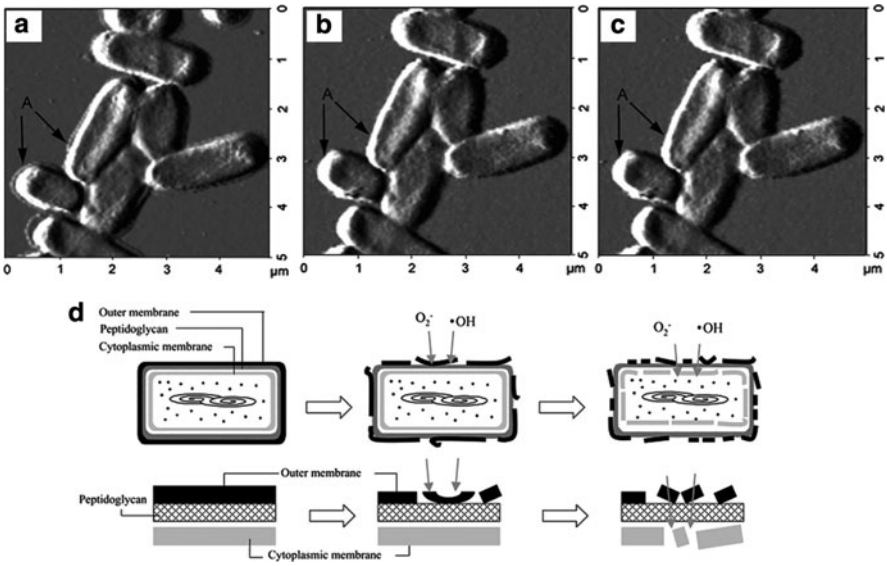

Fig. 15.15 (**a**–**c**) AFM images of *E. coli* cells on the TiO_2 film: (**a**) no illumination, (**b**) illumination for 1 day, (**c**) illumination for 6 days. Light intensity was 1.0 mW/cm^2. (**d**) Schematic illustration of the process of *E. coli* photokilling on TiO_2 film; in the *lower row*, the part of cell envelope was magnified [29]

leading to the peroxidation of the membrane lipid. The structural and functional disordering of the cytoplasmic membrane due to lipid peroxidation led to the loss of cell viability and cell death. And third, decomposition of the dead cell. If the illumination continued for a sufficiently long time, the dead cells were found to be decomposed completely.

As to the CuO-doped TiO_2 film, Sunada et al. [30] presumed that the valence state of the copper played the key role in the bactericidal process both in the dark and under the very weak UV illumination. It has been reported that the copper ions and metallic copper could be transformed into each other by the following redox reaction by the help of photo-generated electrons and holes [92–98].

<Reduction reaction>

$$\begin{aligned} &Cu^{2+} + e^- \rightarrow Cu^+ \\ &Cu^+ + e^- \rightarrow Cu \end{aligned} \tag{15.4}$$

<Oxidation reaction>

$$\begin{aligned} &Cu + h^+ \rightarrow Cu^+ \\ &Cu^+ + h^+ \rightarrow Cu^{2+} \end{aligned} \tag{15.5}$$

Litter et al. [99] and Cieśla et al. [100] reported that the photocatalytic activity of TiO_2 was enhanced through converting photo-generated H_2O_2 into more reactive $^{\cdot}OH$ by the following copper-mediated Fenton-type reactions.

$$\begin{aligned} &H_2O_2 + Cu^+ \rightarrow {}^{\bullet}OH + OH^- + Cu^{2+} \\ &Cu^{2+} + e^- \rightarrow Cu^+ \\ &\text{or} \\ &Cu^{2+} + O_2{}^- \rightarrow Cu^+ + O_2 \end{aligned} \tag{15.6}$$

Sato et al. [40] surmised a possible mechanism of the enhanced antibacterial activity of CuO-doped TiO_2 film, which was associated with photocatalysis under the weak UV illumination (Fig. 15.16). Through a series of photoreactions as expressed above, reactive oxygen species (ROS) such as $^{\cdot}OH$, $^{\cdot}O_2{}^-$ and H_2O_2, were generated by TiO_2 photo-excitation on the CuO-doped TiO_2 film surface. Because H_2O_2 was more stable than $^{\cdot}OH$ and $^{\cdot}O_2{}^-$, it could diffuse from the CuO-doped TiO_2 film surface into the suspension. As shown in Fig. 15.16a, a small amount of copper ion could leach out of the CuO-doped TiO_2 solid phase into the suspension and was reduced into Cu + by receiving electrons from photo-excited TiO_2 nanoparticles. Then, the free Cu + reacted with H_2O_2 to produce $^{\cdot}OH$ via Fenton-type reactions, contributing to the deactivation of microbial cells in the suspension. On the other hand, the following reactions are supposed to occur in solid phase (CuO-doped TiO_2 film) (Fig. 15.16b). Cu^{2+} could be reduced into Cu + by electron from photo-excited TiO_2, and in turn Cu + converted H_2O_2 into

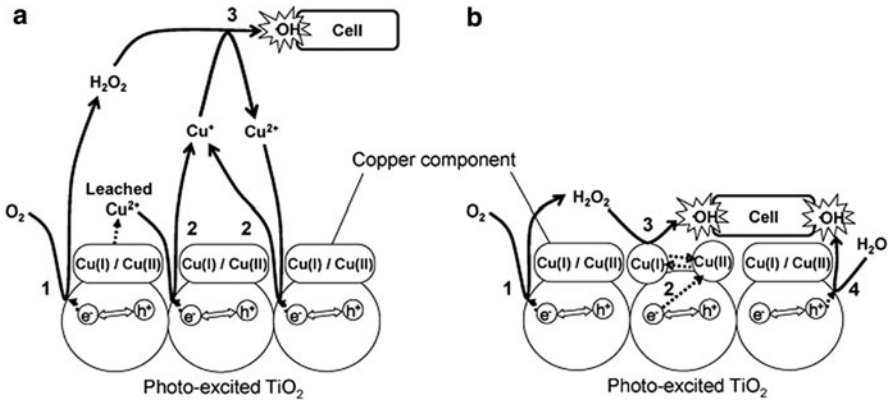

Fig. 15.16 Schematic illustration showing possible mechanism of deactivation on CuO-doped TiO_2 film in the liquid phase (**a**) and on the solid surface (**b**) [40]

·OH, while being oxidized into Cu^{2+} again, leading to much more deactivated bacterial cells. However, Sunada et al. [30] proposed that copper ions could penetrate the damaged membrane into cytoplasm, resulting in a direct disturbance in intracellular metabolic systems, and thus the bactericidal process for the bacterial cells on the CuO-doped TiO_2 film under weak UV illumination consisted of two steps (Fig. 15.17). First, the outer membrane was attacked by the reactive oxygen species produced by TiO_2 photocatalysis and the transformation between Cu^{2+} and Cu^{+} (Fig. 15.17b, c). And then copper ions (maybe and Cu^{+}) were effectively taken into the cytoplasmic membrane (Fig. 15.17c, e). In this case, the photocatalytic reaction mainly played a critical role in assisting the intrusion of copper ions into the cells.

Therefore, the metal nanoparticles may play three roles in killing bacteria: (1) it could prevent photo-generated electrons and holes from surface recombination by trapping of photo-generated electrons with positive metal ions; (2) it increased the yield of hydroxyl radical through the Fenton-type process by reaction with photo-generated H_2O_2, and (3) it diffused into the cytoplasmic membrane of the bacteria and accelerated the lethal effect after the outer membrane of the bacteria was destroyed by oxidizing oxygen species. In addition, the metal ions can kill bacteria directly, which could explain the antibacterial activity of CuO-doped TiO_2 film in the dark.

On the other hand, Akhavan et al. [42] considered that the improved antibacterial property of the MWNTs-doped TiO_2 film could be assigned to the formation of Ti–C and Ti–O–C carbonaceous bonds at 450°C, which was confirmed by the their XPS results. So a possible mechanism of the improvement in the photo-inactivation was proposed (Fig. 15.18b). First, the electrons generated by the photo-excited MWNTs were transmitted to the conduction band of the TiO_2 through the Ti–C bonds, leading to the formation of the positively charged MWNTs, which could capture electrons from the valence band of TiO_2 to generate the holes in the TiO_2 [101, 102]. And the electrons and holes induced the generation of ROS by a series

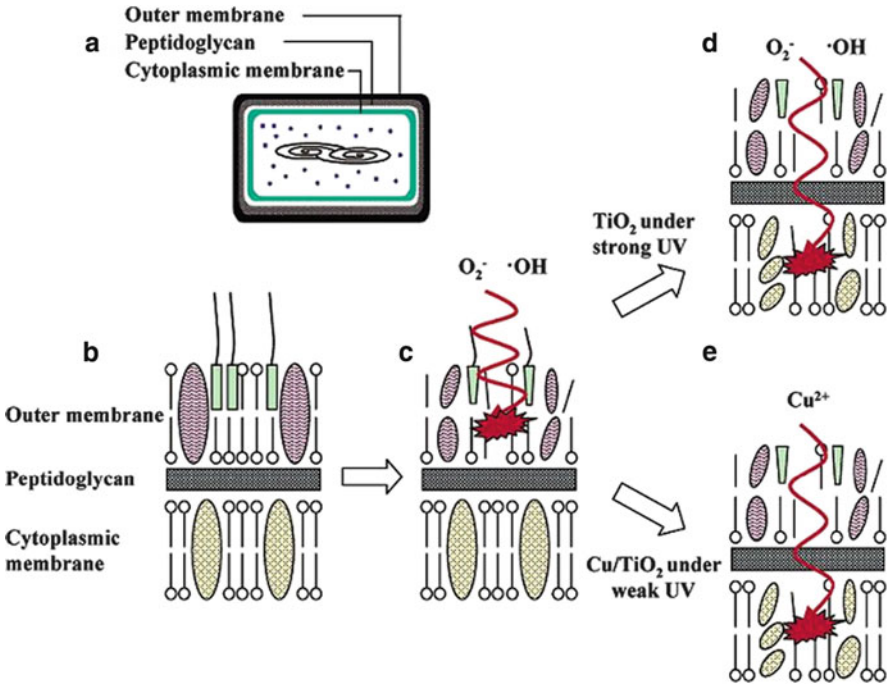

Fig. 15.17 Schematic illustration of the bactericidal process for the copper-resistant *E. coli* cell on the normal TiO_2 film and on the CuO-doped TiO_2 film: (**a**) illustration of *E. coli* cell, (**b**–**e**) enlarged illustration of cell envelope parts [30]

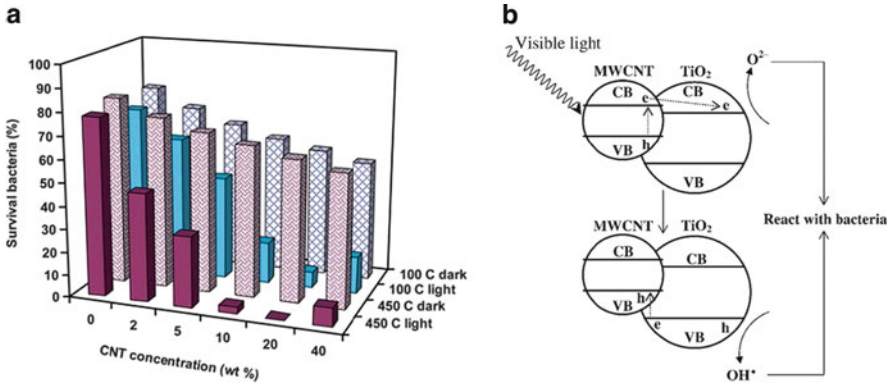

Fig. 15.18 (**a**) Percentage of survival ratio of *E. coli* bacteria on the surface of the MWNTs-doped TiO_2 film annealed at 100°C and 450°C with various MWNTs contents in the dark and under visible light irradiation for 1 h. (**b**) Schematic illustration of photocatalytic mechanism of the MWNTs-doped TiO_2 film under visible light irradiation [42]

of reactions as above described. And second, the formation of the heterojunction between TiO_2 and MWNTs resulted in giving rise to a charge space near the junction to equalize Fermi levels, ranging from several tens to hundreds of nanometres. Not only was the band gap energy within the MWNTs-TiO_2 heterojunction smaller than the band gap energy of the TiO_2 located out of the junction but also a driving force originated from interior electric field of the charge space could separate the photo-generated pairs which resulted in reduction of the recombination rate of the pairs. Additionally, the natural bactericidal activity of MWNTs also contributed to this property in the dark.

15.3.2 ZnO-Based Films

Premanathan et al. [103] suggested that ZnO nanoparticles killed HL 60 cells by generation of ROS and induction of apoptosis. The mechanism of antibacterial activity of ZnO nanoparticles was not well understood although the ZnO nanoparticles could effectively inhibit both Gram-positive and Gram-negative bacteria [104–107].

Antibacterial activity of ZnO nanoparticles may be attributed to several mechanisms. First, by induction of oxidative stress which led to interaction with proteins, DNA, and lipids causing death [108–110]. In 1996, Sawai et al. [107] discovered that H_2O_2 was produced in ZnO slurry and the concentration of H_2O_2 was linearly proportional to the ZnO particles, which confirmed by Yamamoto et al. [111]. It is known that ZnO possesses photocatalytic activity under the UV light [112]. However, most of the antibacterial tests were done under the dark conditions, so it was still not clear how the ROS species were produced and how to improve the active oxygen production in the dark. Second, by membrane destruction due to accumulation of ZnO nanoparticles in the bacterial membrane and also their cellular internalization [113]. Zhang et al. [47] showed that the ZnO nanoparticles damages the membrane of the bacterial cells by the aid of TEM studies, and the electrochemical measurements via a model DOPC monolayer further confirmed the direct interaction between ZnO nanoparticles and the bacterial membrane. And third, by the release of Zn ions that may be responsible for antimicrobial activity by contracting with the membrane of microorganisms [114]. However, the toxicity of ZnO nanoparticles was not directly related to their entering into the cell, rather their intimate contact onto the cell causes changes in the microenvironment in the vicinity of the organism–particle contact area to either increase metal solubilization or to generate ROS [115], which may ultimately damage the cell membrane [116].

15.3.3 AgNPs-Based Films

Although AgNP-based films represented excellent antibacterial activity, the antibacterial mechanism was not completely understood. Generally, it was clear

that the antimicrobial property of silver was related to the amount of silver and the rate of silver released. Silver in its metallic state was inert, but it reacted with moisture, and become ionized. The ionized silver was highly reactive. Silver ions interacted with thiol groups of membrane-bound enzymes and proteins, resulting in membrane structure and permeability changes [117–119]. After penetrating through the cell membrane, silver ions could uncouple the respiratory chain from oxidative phosphorylation [120], and bind to DNA and RNA by denaturing and inhibiting bacterial replication [121].

The antibacterial property of AgNPs-based films was attributed to silver ions generation and unique nanostructure of AgNPs. On the one hand, Akhavan et al. [51] demonstrated that silver ions were released over long periods from the film surface, even from TiO_2-capped AuNPs and silver nanorods films (Fig. 15.19) [65]. Agarwal et al. [122] also found that localization of AgNPs on the AgNPs/poly (allylamine hydrochloride)/poly (acrylic acid) film generated the concentrations of silver ions required for antibacterial activity at the surface, without requiring the high loading of silver AgNPs. On the other hand, free AgNPs released from films could directly interact with the microorganism by disrupting/penetrating the cell envelope, and generating reactive oxygen species (ROS) [108, 109] that caused deadly damage. Moreover, free AgNPs preferentially attacked the respiratory chain, cell division finally leading to cell death [123, 124]. So, compared to silver ions, the effective concentration of AgNPs was ~10^3-fold lower, being at the nanomolar level [125]. In the AgNPs-based composite film, the improvement of antibacterial activity also partly arose from the action of the other components, such as AgNPs/TiO_2 films [126] and AgNPs/ZnO film [127].

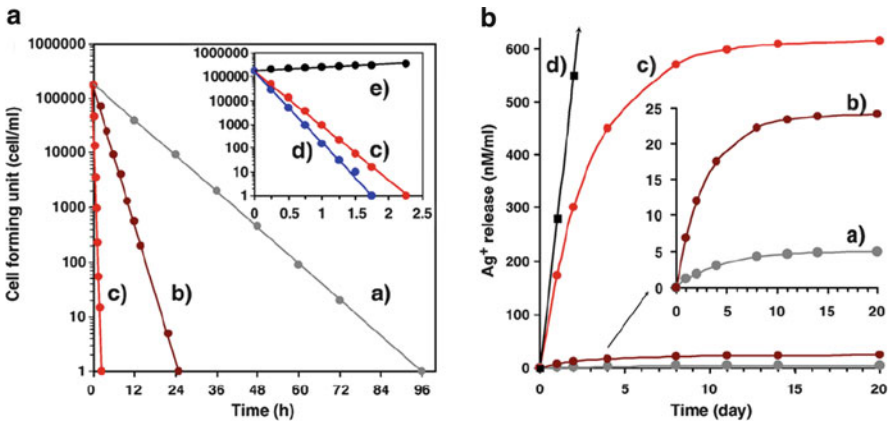

Fig. 15.19 (**a**) CFU of *E. coli* cultured for various periods in the medium containing different films. (**b**) The silver ion release curves of the TiO2-capped AgNPa and silver nanorods films. (**a**) TiO_2-capped Ag film in the dark. (**b**) TiO_2-capped AgNPs film in the dark. (**c**) TiO_2-capped silver nanorods film in the dark. (**d**) Silver nanorods film in the dark. In the *inset* of (**a**): TiO_2-capped silver nanorods film in the dark (**c**) and under UV irradiation (**d**); (**e**) blank sample [65]

15.3.4 CNTs-Based Films

Despite agreement about the potential toxicity of CNTs on mammalian cells, the mechanism of CNTs toxicity is still elusive. Previous studies have proposed three hypothesized mechanisms: oxidative stress [128, 129], metal toxicity [130, 131], and physical piercing causing rupture [68, 132]. where the generation of reactive oxygen species (ROS) and oxidative stress are the most developed paradigms for the mechanism of CNTs cytotoxicity. However, how do CNTs exert their antimicrobial activity? Two possible mechanisms have been proposed, i.e. mechanical disruption, where nanotubes act to physically pierce or otherwise perturb the bacterial membrane, and oxidative stress, where the high reductive potential of nanoscale carbon induced the generation of ROS to damage cell membranes and to disturb the metabolic pathway.

Kang et al. [69] and Brady-Estévez et al. [71] studied the scanning electron microscopic (SEM) images of CNTs-treated *E. coli*, and found that the treated *E. coli* cells became flattened, and lost their cellular integrity, suggesting irreversible cell membrane damage and cell death (Fig. 15.20), which confirmed that the antibacterial activity of CNTs was related to the surface characteristics of the bacteria [14]. The toxicity of CNTs against Gram-positive bacteria was smaller than that of CNTs against Gram-negative bacteria, owing to the thicker peptidoglycan in Gram-positive bacterial cell walls [133]. In 2008, Kang et al. [134] further found that the cytoplasmic nucleic acids were presented in the culture medium by DNA and RNA assays, and that genes related to the cell envelope integrity, including fatty acid biosynthesis, Tol/Pal system [135–137], and PhoPQ two-component system [138], were up-regulated in the SWNTs-treated *E. coli*, confirming the cell membrane damage. However, another kind of gene related to oxidative stress (e.g. *soxRS*, *oxyR*) was up-regulated in the DNA micro-array analysis, suggesting that oxidative stress was also responsible for the antibacterial property of CNTs.

Therefore, a three-step interaction process between CNTs and bacteria was proposed. First, by initial CNTs–bacteria contact. The bacteria were deposited

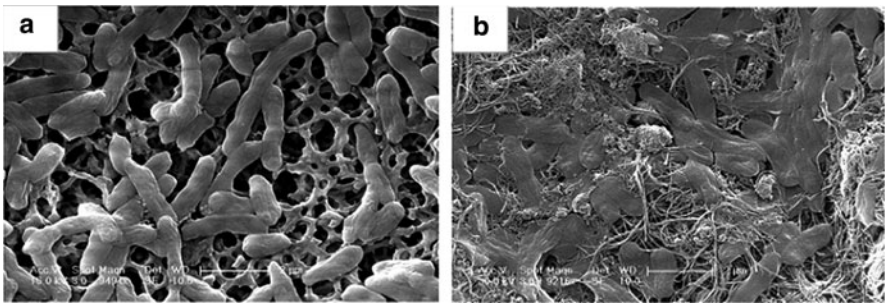

Fig. 15.20 SEM images of *E. coli* incubated for 60 min without (**a**) and with (**b**) SWNTs. The cell membrane of treated *E. coli* was damaged, leading to cell death [69]

onto CNTs resulting in direct bacteria–CNTs contact which could be mediated by the exposed CNTs surface area, bacteria concentration, and solution composition. Second, by perturbation of the cell membrane. The mechanism of this step could be clarified according to the toxicity of various classes of hydrocarbons against aquatic microorganisms [139]. The toxicity of hydrocarbons involved two parts: the nonspecific and specific toxicity. The nonspecific toxicity was the disruption of the cell membrane, and dependent on the hydrophobicity of hydrocarbon. And the specific toxicity was described as how the hydrocarbons affected membrane proton transport, disrupted specific proteins, or chemically oxidized biomolecules (i.e. proteins, lipids, and DNA), which was attributed to the electrophilicity of hydrocarbon [140, 141]. Furthermore, Kang et al. [73] demonstrated that the perturbation of cell membrane was related to diameter and hydrophobicity of CNTs, the intensity of the open tube ends. And third, by bacterial oxidation. The cell death resulted from the ROS oxidation and regulation of cellular metabolic pathway (Fig. 15.21). The ROS were generated by the cell membrane damage and the interactions between CNTs and biomolecules (e.g., GSH [75]).

Vecitis et al. [80] proposed two primary mechanisms of electrochemical inactivation of *E. coli* and MS2: the direct oxidation of pathogen in contact with the MWNTs anode, and the indirect oxidation of pathogen via anodic production of an aqueous oxidant (e.g., $Cl_2^{\cdot -}$, $HO^{\cdot}$, or $SO_4^{\cdot 2-}$). During the process, MWNTs provided positive holes (h^+). The oxidation reaction of pathogen with MWNTs and anodic one-electron oxidant resulted in the cell membrane damage and cell death, further confirmed by the SEM images of different potential-treated *E. coli*.

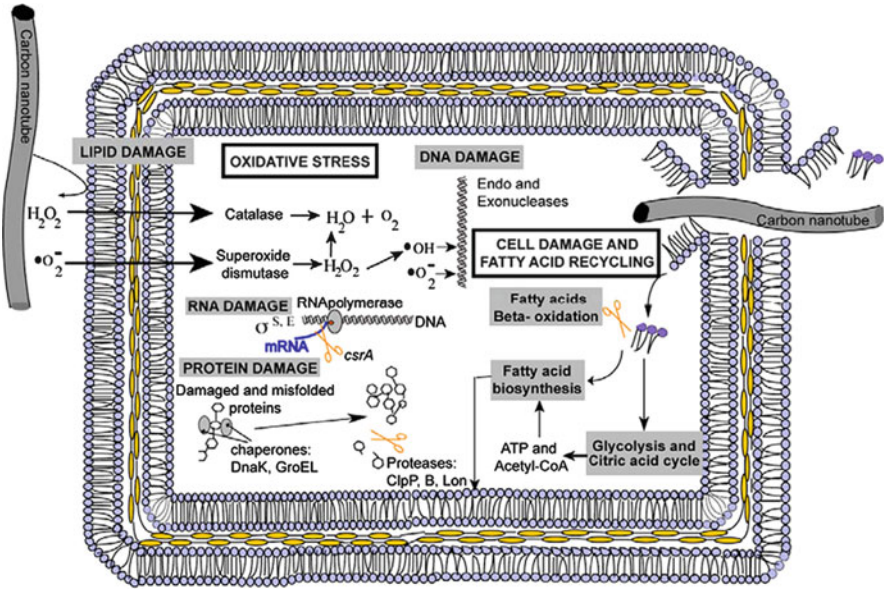

Fig. 15.21 Schematic summary of *E. coli* K12 gene expression stress responses under exposure to SWNTs and MWNTs, suggesting the mechanism of CNTs-induced anbacterial activity [73]

15.3.5 Graphene-Based Films

The antibacterial mechanism of graphene-based paper was attributed to graphene-induced cell membrane damage after interactions between graphene derivatives and bacterial cells. Akhavan et al. [87] reported that concentrations of RNA in the solutions of the bacteria exposed to the both GO nano-walls and rGO nano-walls were meaningfully higher than that of the control sample (Fig. 15.22a, b), suggesting the bacteria membrane damage. And the SEM images of *E. coli* attached on the surfaces of GO and rGO papers showed that treated *E. coli* cells on the paper lost the integrity of membranes (Fig. 15.22c, d) [11], further confirming this hypothesis. Additionally, in the tween/rGO composite paper, the tween-20 could prevent bacteria from adhering on the paper owing to its amphiphilic property [88].

15.4 Toxicity of Nanomaterial-Based Films

With the development of nanotechnology, artificial nanomaterials meeting different requirements were designed and applied. As a result, the biological effects of these artificial nanomaterials on humans and the environment became more and more

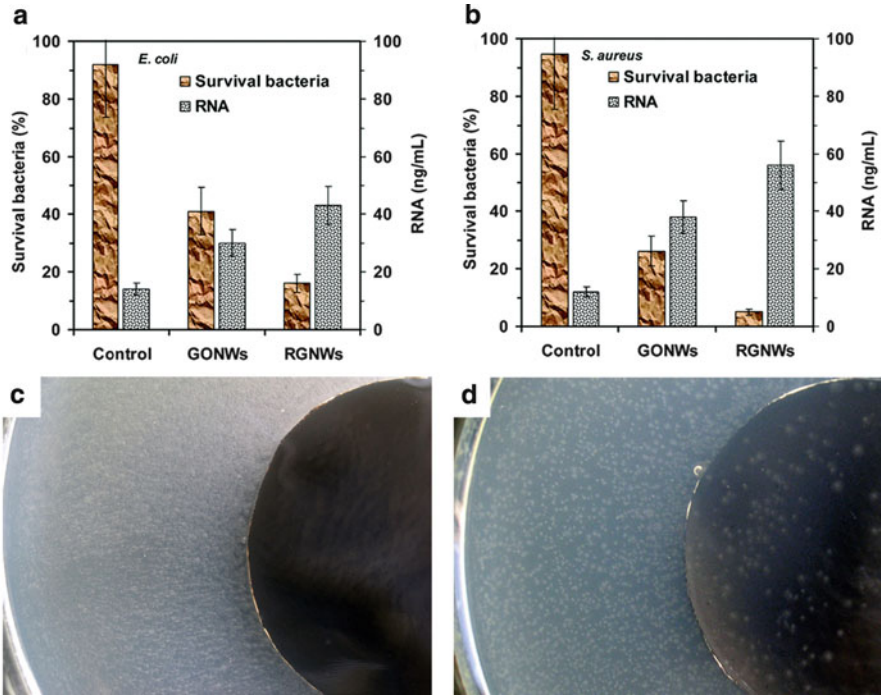

Fig. 15.22 (**a**, **b**) Cytotoxicity of GO nanowalls and rGO nanowalls to *E. coli* (**a**) and *S. aureus* (**b**), and concentrations of RNA in the PBS of the bacteria exposed to the nanowalls [87]. (**c**, **d**) Photographs of *E. coli* growth on GO (**c**) and rGO (**d**) paper (overnight incubation at 37°C) [11]

important. Owing to differences in test methods, the biological effect of the same nanomaterial was not always in agreement. However, it was known that high concentration of nanomaterials was toxic to mammalian cells.

Lagopati et al. [26] reported that TiO_2 nanoparticles could kill the mammalian cells via reactive oxygen species generated by photocatalysis, while Kommireddy et al. [142] revealed that TiO_2 thin film could speed the spread of mouse mesenchymal stem cells owing to the rough surface. The published literature shows that ZnO nanoparticles have been applied to drug delivery and cosmetics with nontoxicity [143], while Hanley et al. [144] demonstrated that ZnO nanoparticles could kill cancerous T cells owing to the generation of ROS. Huang et al. [145] also reported the cytotoxicity of ZnO nanoparticles with the size of 20 nm against human bronchial epithelial cells (BEAS-2B) was concentration- and time-dependent, resulting from elevating oxidative stress, disturbing calcium homeostasis and causing membrane damage. However, ZnO nanoparticles were considered and generally recognized as safe (GRAS) material by FDA [146].

Although silver could effectively suppress the growth of microorganisms, it also led to dose-related toxicity in tissue. It has been reported that silver ions accumulated in epithelial cells, macrophages, fibroblasts, and connective tissue [147, 148] and caused tissue toxicity and impaired wound healing [149, 150]. In vitro studies have also demonstrated that the concentrations of silver released from AgNPs-based film could be cytotoxic to mammalian cells involved in wound healing, including fibroblasts [151, 152], keratinocytes [151], and lymphocytes [153]. However, it was found that human osteoblast attached and grew well on the surface containing AgNPs [154, 155]. Agarwal et al. [122] employed molecularly thin polymeric films [poly (allylamine hydrochloride) and poly (acrylic acid)] prepared by layer-by-layer deposition to localize AgNPs on surfaces, and found that the resulting composite film could release silver ions, leading to antibacterial activity without cytotoxicity. Also, Zan et al. [63] considered that the high resistance of AgNPs/poly (vinyl alcohol)/ploy (L-lactic acid) film to HeLa cells is not due to the embedded AgNPs, but to its high water content, hydrophilicity, and low interfacial tension between the hydrogel surface and the surrounding fluids.

Generally speaking, carbon-based nanomaterials were regarded as “safe” since the carbon element was inherently compatible with living systems. However, the high concentrations of CNTs and graphene derivatives were cytotoxic to the mammalian cells [132, 133], and the cytotoxicity could be mitigated by chemical modification [156–158]. Agarwal et al. [159] demonstrated that SWNTs thin film inhibits the proliferation, viability, and neurogenesis of PC 12 cells, and the proliferation of osteoblasts. The CNTs films can improve neural signal transfer [160]. The tendency of graphene oxide cytotoxicity was similar to that of CNTs cytotoxicity [161]. Agarwal et al. [159] and Chen et al. [162] showed that graphene-based paper displayed good biocompatibility against neuroendocrine PC 12 cells, osteoblast, and mouse fibroblast cell line L-929. Park et al. [88] also demonstrated that tween/rGO paper showed no cytotoxicity against African green monkey kidney cells, embryonic bovine cells, and Crandell Rees feline kidney cells.

15.5 Applications of Nanomaterial-Based Films

Despite the considerable concerns on public health and food safety, antibacterial materials have become more and more important in everyday use. However, traditional antibacterial materials have raised significant concerns on antibiotic resistance, environmental pollution, relatively complex processing and high cost [163, 164]. Owing to their excellent antibacterial property, nanomaterials-based films can inactivate bacteria attached on the surface, and thus nanomaterial-based films have been extensively applied to self-sterilizing surfaces of materials in public locations, food storage and clinical facilities, such as hospitals, elderly care facilities, wound care dressings, and orthopedic implants, where it was critical to control the surface and airborne bacteria.

Antimicrobial food packaging materials have been used to extend the lag phase and reduce the growth rate of microorganisms in order to extend shelf life and to maintain product quality and safety. Emamifar et al. [95] used AgNPs/LDPE and ZnO/LDPE films to store orange juice at 4 °C for 112 days, and found that the films could significantly suppress the growth of *Lactobacillus plantarum* in the orange juice, suggesting promising applications of nanomaterial-based film in food packaging.

Fujishima et al. [37] developed antibacterial tiles by covering ordinary tiles with TiO_2-Cu composite film, and tested such tiles on the floor and walls of the hospital operating room. The results showed that the bacterial counts decreased to negligible levels in a period of 1 h, and surprisingly, the bacterial counts in the surrounding air also significantly decreased, leading to commercial applications of such tiles in hospitals, hotels, and restaurants, among others [22]. Ohko et al. [121] fabricated TiO_2 film-coated silicone catheters, with repeated bending and resistibility to scratching. Further clinical studies showed TiO_2 film-coated silicone catheters presented better antibacterial activity compared to conventional catheters, suggesting the promising clinical application as an alternative to conventional catheters [165].

15.6 Conclusions

Recently, microorganism safety has attracted increasing attention. Particularly, the Severe Acute Respiratory Syndromes (SARS) virus, H1N1 flu virus and superbacteria are seriously endangering people's health. The development of new nanomaterial-based antibacterial paper may provide a unique solution. In this chapter, we have summarized the preparation, antibacterial activity, and mechanisms, as well as potential applications, of nanomaterial-based paper. Although there still exist many challenges, such as the high cost, complex synthesis process, and environmental impact, we have witnessed significant advances toward the design and fabrication of novel antibacterial materials that may eventually find real-world applications.

References

1. Ip M, Lui SL, Poon VKM, Lung I, Burd A (2006) Antimicrobial activities of silver dressings: an *in vitro* comparison. J Med Microbiol 55:59–63
2. Mai L, Huang C, Wang D, Zhang Z, Wang Y (2009) Effect of C doping on the structural and optical properties of sol-gel TiO_2 thin films. Appl Surf Sci 255:9285–9289
3. Cheng TC, Chang CY, Chang CI, Hwang CJ, Hsu HC, Wang DY, Yao KS (2008) Photocatalytic bactericidal effect of TiO_2 film on fish pathogens. Surf Coat Technol 203:925–927
4. Mai L, Wang D, Zhang S, Xie Y, Huang C, Zhang Z (2010) Synthesis and bactericidal ability of Ag/TiO_2 composite films deposited on titanium plate. Appl Surf Sci 257:974–978
5. Yu BY, Leung KM, Guo QQ, Lau WM, Yang J (2011) Synthesis of Ag-TiO_2 composite nano thin film for antimicrobial application. Nanotechnology 22:115603
6. Kingery WD, Bowen HK, Uhlmann DR (1976) Introduction to Ceramics. Wiley, New York
7. Kim K, Lee HB, Lee JW, Shin KS (2010) Poly(ethylenimine)-stabilized silver nanoparticles assembled into 2-dimensional arrays at water-toluene interface. J Colloid Interface Sci 345:103–108
8. Liao YA, Wang YQ, Feng XX, Wang WC, Xu FJ, Zhang LQ (2010) Antibacterial surfaces through dopamine functionalization and silver nanoparticle immobilization. Mater Chem Phys 121:534–540
9. Lee SM, Lee BS, Byun TG, Song KC (2010) Preparation and antibacterial activity of silver-doped organic-inorganic hybrid coatings on glass substrates. Colloid Surf A-Physicochem Eng Asp 355:167–171
10. Fu JH, Ji J, Fan DZ, Shen JC (2006) Construction of antibacterial multilayer films containing nanosilver *via* layer-by-layer assembly of heparin and chitosan-silver ions complex. J Biomed Mater Res Part A 79A:665–674
11. Hu W, Peng C, Luo W, Lv M, Li X, Li D, Huang Q, Fan C (2010) Graphene-based antibacterial paper. ACS Nano 4:4317–4323
12. Hummers WS, Offeman RE (1958) Preparation of graphitic oxide. J Am Chem Soc 80:1339
13. Stankovich S, Dikin DA, Piner RD, Kohlhaas KA, Kleinhammes A, Jia Y, Wu Y, Nguyen ST, Ruoff RS (2007) Synthesis of graphene-based nanosheets via chemical reduction of exfoliated graphite oxide. Carbon 45:1558–1565
14. Brady-Estévez AS, Schnoor MH, Kang S, Elimelech M (2010) SWNT − MWNT hybrid filter attains high viral removal and bacterial inactivation. Langmuir 26:19153–19158
15. Schiffman JD, Elimelech M (2011) Antibacterial activity of electrospun polymer mats with incorporated narrow diameter single-walled carbon nanotubes. ACS Appl Mater Interfaces 3:462–468
16. Chen Q, Yue L, Xie FY, Zhou ML, Fu YB, Zhang YF, Weng J (2008) Preferential facet of nanocrystalline silver embedded in polyethylene oxide nanocomposite and its antibiotic behaviors. J Phys Chem C 112:10004–10007
17. Gordon R (1997) Chemical vapor deposition of coatings on glass. J Noncryst Solids 218:81–91
18. Yates HM, Brook LA, Ditta IB, Evans P, Foster HA, Sheel DW, Steele A (2008) Photo-induced self-cleaning and biocidal behaviour of titania and copper oxide multilayers. J Photochem Photobiol Chem 197:197–205
19. Davis MJ, Benito G, Sheel DW, Pemble ME (2004) Growth of thin films of molybdenum and tungsten oxides by combustion CVD using aqueous precursor solutions. Chem Vapor Depos 10:29–34
20. Reyes-Coronado D, Rodríguez-Gattorno G, Espinosa-Pesqueira M, Cab C, de Coss R, Oskam G (2008) Phase-pure TiO_2 nanoparticles: anatase, brookite and rutile. Nanotechnology 19:145605
21. Fujishima A (1972) Electrochemical photolysis of water at a semiconductor electrode. Nature 238:37–38

22. Fujishima A, Zhang X, Tryk DA (2008) TiO_2 photocatalysis and related surface phenomena. Surf Sci Rep 63:515–582
23. Matsunaga T, Tomoda R, Nakajima T, Wake H (1985) Photoelectrochemical sterilization of microbial cells by semiconductor powders. FEMS Microbiol Lett 29:211–214
24. Ogino C, Shibata N, Sasai R, Takaki K, Miyachi Y, Kuroda S, Ninomiya K, Shimizu N (2010) Construction of protein-modified TiO_2 nanoparticles for use with ultrasound irradiation in a novel cell injuring method. Bioorg Med Chem Lett 20:5320–5325
25. Fujishima A, Rao TN, Tryk DA (2000) Titanium dioxide photocatalysis. J Photochem Photobiol C Photochem Rev 1:1–21
26. Lagopati N, Kitsiou PV, Kontos AI, Venieratos P, Kotsopoulou E, Kontos AG, Dionysiou DD, Pispas S, Tsilibary EC, Falaras P (2010) Photo-induced treatment of breast epithelial cancer cells using nanostructured titanium dioxide solution. J Photochem Photobiol Chem 214:215–223
27. Matsui K, Segawa M, Tanaka T, Kondo A, Ogino C (2009) Antibody-immobilized TiO_2 nanoparticles for cancer therapy. J Biosci Bioeng 108:S36-S37
28. McCullagh C, Robertson JMC, Bahnemann DW, Robertson PKJ (2007) The application of TiO_2 photocatalysis for disinfection of water contaminated with pathogenic micro-organisms: a review. Res Chem Intermed 33:359–375
29. Sunada K, Watanabe T, Hashimoto K (2003) Studies on photokilling of bacteria on TiO_2 thin film. J Photochem Photobiol Chem 156:227–233
30. Sunada K, Watanabe T, Hashimoto K (2003) Bactericidal activity of copper-deposited TiO_2 thin film under weak UV light illumination. Environ Sci Technol 37:4785–4789
31. Dai K, Peng T, Ke D, Wei B (2009) Photocatalytic hydrogen generation using a nanocomposite of multi-walled carbon nanotubes and TiO_2 nanoparticles under visible light irradiation. Nanotechnology 20:125603
32. Akhavan O, Azimirad R, Safa S, Larijani MM (2010) Visible light photo-induced antibacterial activity of CNT-doped TiO_2 thin films with various CNT contents. J Mater Chem 20:7386–7392
33. Foster HA, Sheel DW, Sheel P, Evans P, Varghese S, Rutschke N, Yates HM (2010) Antimicrobial activity of titania/silver and titania/copper films prepared by CVD. J Photochem Photobiol Chem 216:283–289
34. Kikuchi Y, Sunada K, Iyoda T, Hashimoto K, Fujishima A (1997) Photocatalytic bactericidal effect of TiO_2 thin films: dynamic view of the active oxygen species responsible for the effect. J Photochem Photobiol Chem 106:51–56
35. Wei C, Lin WY, Zainal Z, Williams NE, Zhu K, Kruzic AP, Smith RL, Rajeshwar K (1994) Bactericidal activity of TiO_2 photocatalyst in aqueous media: toward a solar-assisted water disinfection system. Environ Sci Technol 28:934–938
36. Watts RJ, Kong S, Orr MP, Miller GC, Henry BE (1995) Photocatalytic inactivation of coliform bacteria and viruses in secondary wastewater effluent. Water Res 29:95–100
37. Fujishima A, Hashimoto T, Watanabe T (1999) TiO_2 Photocatalysis: Fundamentals and Applications. BKC, Inc., Tokyo
38. Zhang QJ, Sun CH, Zhao Y, Zhou SY, Hu XJ, Chen P (2010) Low Ag-doped titanium dioxide nanosheet films with outstanding antimicrobial property. Environ Sci Technol 44:8270–8275
39. Ondok V, Musil J, Meissner M, Čerstvý R, Fajfrík K (2010) Two-functional DC sputtered Cu-containing TiO_2 thin films. J Photochem Photobiol Chem 209:158–162
40. Sato T, Taya M (2006) Copper-aided photosterilization of microbial cells on TiO_2 film under irradiation from a white light fluorescent lamp. Biochem Eng J 30:199–204
41. Akhavan O, Abdolahad M, Abdi Y, Mohajerzadeh S (2009) Synthesis of titania/carbon nanotube heterojunction arrays for photoinactivation of *E. coli* in visible light irradiation. Carbon 47:3280–3287
42. Oh WC, Jung AR, Ko WB (2009) Characterization and relative photonic efficiencies of a new nanocarbon/TiO_2 composite photocatalyst designed for organic dye decomposition and bactericidal activity. Mater Sci Eng C 29:1338–1347

43. Brook LA, Evans P, Foster HA, Pemble ME, Steele A, Sheel DW, Yates HM (2007) Highly bioactive silver and silver/titania composite films grown by chemical vapour deposition. J Photochem Photobiol Chem 187:53–63
44. Watanabe T, Hashimoto K, Fujishima A, Presented at the 1st International Conference on TiO_2 Photocatalytic Purification and Treatment of Water and Air, Toronto & Ontario,1992.
45. Wang R, Hashimoto K, Fujishima A, Chikuni M, Kojima E, Kitamura A, Shimohigoshi M, Watanabe T (1998) Photogeneration of highly amphiphilic TiO_2 surfaces. Adv Mater 10:135–138
46. Padmavathy N, Vijayaraghavan R (2008) Enhanced bioactivity of ZnO nanoparticles-an antimicrobial study. Sci Technol Adv Mater 9:035004
47. Zhang L, Jiang Y, Ding Y, Povey M, York D (2007) Investigation into the antibacterial behaviour of suspensions of ZnO nanoparticles (ZnO nanofluids). J Nanopart Res 9:479–489
48. Chandramouleeswaran S, Mhaske ST, Kathe AA, Varadarajan PV, Prasad V, Vigneshwaran N (2007) Functional behaviour of polypropylene/ZnO-soluble starch nanocomposites. Nanotechnology 18:385702
49. Shalumon KT, Anulekha KH, Nair SV, Nair SV, Chennazhi KP, Jayakumar R (2011) Sodium alginate/poly(vinyl alcohol)/nano ZnO composite nanofibers for antibacterial wound dressings. Int J Biol Macromol. DOI: 10.1016/j.ijbiomac.2011.04.005
50. Silver S (2003) Bacterial silver resistance: molecular biology and uses and misuses of silver compounds. FEMS Microbiol Rev 27:341–353
51. Akhavan O, Ghaderi E (2009) Bactericidal effects of Ag nanoparticles immobilized on surface of SiO_2 thin film with high concentration. Curr Appl Phys 9:1381–1385
52. Baker C, Pradhan A, Pakstis L, Pochan DJ, S.I. S (2005) Synthesis and antibacterial properties of silver nanoparticles. J Nanosci Nanotechnol 5:244–249
53. Ohko Y, Tatsuma T, Fujii T, Naoi K, Niwa C, Kubota Y, Fujishima A (2003) Multicolour photochromism of TiO_2 films loaded with silver nanoparticles. Nat Mater 2:29–31
54. Akhavan O (2009) Lasting antibacterial activities of Ag-TiO_2/Ag/a-TiO_2 nanocomposite thin film photocatalysts under solar light irradiation. J Colloid Interface Sci 336:117–124
55. Rhim JW, Hong SI, Park HM, Ng PKW (2006) Preparation and characterization of chitosan-based nanocomposite films with antimicrobial activity. J Agric Food Chem 54:5814–5822
56. Tankhiwale R, Bajpai SK (2010) Silver-nanoparticle-loaded chitosan lactate films with fair antibacterial properties. J Appl Polym Sci 115:1894–1900
57. Yoksan R, Chirachanchai S (2010) Silver nanoparticle-loaded chitosan-starch based films: fabrication and evaluation of tensile, barrier and antimicrobial properties. Mater Sci Eng C 30:891–897
58. Cui XQ, Li CM, Bao HF, Zheng XT, Lu ZS (2008) *In situ* fabrication of silver nanoarrays in hyaluronan/PDDA layer-by-layer assembled structure. J Colloid Interface Sci 327:459–465
59. Fayaz AM, Balaji K, Girilal M, Kalaichelvan PT, Venkatesan R (2009) Mycobased synthesis of silver nanoparticles and their incorporation into sodium alginate films for vegetable and fruit preservation. J Agric Food Chem 57:6246–6252
60. Dong G, Xiao X, Liu X, Qian B, Liao Y, Wang C, Chen D, Qiu J (2009) Functional Ag porous films prepared by electrospinning. Appl Surf Sci 255:7623–7626
61. Jiang SX, Qin WF, Guo RH, Zhang L (2010) Surface functionalization of nanostructured silver-coated polyester fabric by magnetron sputtering. Surf Coat Technol 204:3662–3667
62. Vasilev K, Sah VR, Goreham RV, Ndi C, Short RD, Griesser HJ (2010) Antibacterial surfaces by adsorptive binding of polyvinyl-sulphonate-stabilized silver nanoparticles. Nanotechnology 21:215102
63. Zan X, Kozlov M, McCarthy TJ, Su Z (2010) Covalently attached, silver-doped poly(vinyl alcohol) hydrogel films on poly(L-lactic acid). Biomacromolecules 11:1082–1088
64. Yliniemi K, Vahvaselka M, Van Ingelgem Y, Baert K, Wilson BP, Terryn H, Kontturi K (2008) The formation and characterisation of ultra-thin films containing Ag nanoparticles. J Mater Chem 18:199–206
65. Akhavan O, Ghaderi E (2009) Capping antibacterial Ag nanorods aligned on Ti interlayer by mesoporous TiO_2 layer. Surf Coat Technol 203:3123–3128

66. Vimala K, Mohan YM, Sivudu KS, Varaprasad K, Ravindra S, Reddy NN, Padma Y, Sreedhar B, MohanaRaju K (2010) Fabrication of porous chitosan films impregnated with silver nanoparticles: a facile approach for superior antibacterial application. Colloid Surf B-Biointerfaces 76:248–258
67. Lu F, Gu L, Meziani MJ, Xin W, Luo PG, Veca LM, Cao L, Sun Y-P (2009) Advances in bioapplications of carbon nanotubes. Adv Mater 21:139–152
68. Narayan RJ, Berry CJ, Brigmon RL (2005) Structural and biological properties of carbon nanotube composite films. Mater Sci Eng B 123:123–129
69. Kang S, Pinault M, Pfefferle LD, Elimelech M (2007) Single-walled carbon nanotubes exhibit strong antimicrobial activity. Langmuir 23:8670–8673
70. Rodrigues DF, Elimelech M (2010) Toxic effects of single-walled carbon nanotubes in the development of *E. coli* biofilm. Environ Sci Technol 44:4583–4589
71. Brady-Estévez AS, Kang S, Elimelech M (2008) A single-walled-carbon-nanotube filter for removal of viral and bacterial pathogens. Small 4:481–484
72. Kang S, Mauter MS, Elimelech M (2009) Microbial cytotoxicity of carbon-based nanomaterials: implications for river water and wastewater effluent. Environ Sci Technol 43:2648–2653
73. Kang S, Mauter MS, Elimelech M (2008) Physicochemical determinants of multiwalled carbon nanotube bacterial cytotoxicity. Environ Sci Technol 42:7528–7534
74. Yang C, Mamouni J, Tang Y, Yang L (2010) Antimicrobial activity of single-walled carbon nanotubes: Length effect. Langmuir 26:16013–16019
75. Vecitis CD, Zodrow KR, Kang S, Elimelech M (2010) Electronic-structure-dependent bacterial cytotoxicity of single-walled carbon nanotubes. ACS Nano 4:5471–5479
76. Simmons TJ, Lee SH, Park TJ, Hashim DP, Ajayan PM, Linhardt RJ (2009) Antiseptic single wall carbon nanotube bandages. Carbon 47:1561–1564
77. Aslan S, Loebick CZ, Kang S, Elimelech M, Pfefferle LD, Van Tassel PR (2010) Antimicrobial biomaterials based on carbon nanotubes dispersed in poly(lactic-co-glycolic acid). Nanoscale 2:1789–1794
78. Pangule RC, Brooks SJ, Dinu CZ, Bale SS, Salmon SL, Zhu GY, Metzger DW, Kane RS, Dordick JS (2010) Antistaphylococcal nanocomposite films based on enzyme-nanotube conjugates. ACS Nano 4:3993–4000
79. Zhou J, Qi X (2011) Multi-walled carbon nanotubes/epilson-polylysine nanocomposite with enhanced antibacterial activity. Lett Appl Microbiol 52:76–83
80. Vecitis CD, Schnoor MH, Rahaman MS, Schiffman JD, Elimelech M (2011) Electrochemical multiwalled carbon nanotube filter for viral and bacterial removal and inactivation. Environ Sci Technol 45:3672–3679
81. Novoselov KS, Geim AK, Morozov SV, Jiang D, Zhang Y, Dubonos SV, Grigorieva IV, Firsov AA (2004) Electric field effect in atomically thin carbon films. Science 306:666–669
82. Stankovich S, Dikin DA, Dommett GHB, Kohlhaas KM, Zimney EJ, Stach EA, Piner RD, Nguyen ST, Ruoff RS (2006) Graphene-based composite materials. Nature 442:282–286
83. Geim AK (2009) Graphene: status and prospects. Science 324:1530–1534
84. Lin YM, Dimitrakopoulos C, Jenkins KA, Farmer DB, Chiu HY, Grill A, Avouris P (2010) 100-GHz transistors from wafer-scale epitaxial graphene. Science 327:662
85. Schedin F, Geim AK, Morozov SV, Hill EW, Blake P, Katsnelson MI, Novoselov KS (2007) Detection of individual gas molecules adsorbed on graphene. Nat Mater 6:652–655
86. Wang X, Zhi L, Tsao N, Tomović Ž, Li J, Müllen K (2008) Transparent carbon films as electrodes in organic solar cells. Angew Chem Int Ed 47:2990–2992
87. Akhavan O, Ghaderi E (2010) Toxicity of graphene and graphene oxide nanowalls against bacteria. ACS Nano 4:5731–5736
88. Park S, Mohanty N, Suk JW, Nagaraja A, An J, Piner RD, Cai W, Dreyer DR, Berry V, Ruoff RS (2010) Biocompatible, robust free-standing paper composed of a tween/graphene composite. Adv Mater 22:1736–1740
89. Hoffmann MR, Martin ST, Choi W, Bahnemann DW (1995) Environmental applications of semiconductor photocatalysis. Chem Rev 95:69–96

90. Ishibashi K, Fujishima A, Watanabe T, Hashimoto K (2000) Generation and deactivation processes of superoxide formed on TiO_2 film illuminated by very weak UV light in air or water. J Phys Chem B 104:4934–4938
91. Kühn KP, Chaberny IF, Massholder K, Stickler M, Benz VW, Sonntag H-G, Erdinger L (2003) Disinfection of surfaces by photocatalytic oxidation with titanium dioxide and UVA light. Chemosphere 53:71–77
92. Fujihira M, Satoh Y, Osa T (1982) Heterogeneous photocatalytic reactions on semiconductor materials. III. effect of pH and Cu^{2+} ions on the photo-fenton type reaction. Bull Chem Soc Jpn 55:666–671
93. Ward MD, Bard AJ (1982) Photocurrent enhancement via trapping of photogenerated electrons of titanium dioxide particles. J Phys Chem 86:3599–3605
94. Okamoto K, Yamamoto Y, Tanaka H, Tanaka M, Itaya A (1985) Heterogeneous photocatalytic decomposition of phenol over TiO2 powder. Bull Chem Soc Jpn 58:2015–2022
95. Wei TY, Wang YY, Wan CC (1990) Photocatalytic oxidation of phenol in the presence of hydrogen peroxide and titanium dioxide powders. J Photochem Photobiol Chem 55:115–126
96. Zang L, Liu CY, Ren XM (1995) Photochemistry of semiconductor particles. Part 4.-Effects of surface condition on the photodegradation of 2,4-dichlorophenol catalysed by TiO_2 suspensions. J Chem Soc Faraday Trans 91:917–923
97. Zhu H, Zhang M, Xia Z, Gary LKC (1995) Titanium dioxide mediated photocatalytic degradation of monocrotophos. Water Res 29:2681–2688
98. Brezová V, Blažková Ab, Borošová E, Čeppan M, Fiala R (1995) The influence of dissolved metal ions on the photocatalytic degradation of phenol in aqueous TiO2 suspensions. J Mol Catal Chem 98:109–116
99. Litter MI (1999) Heterogeneous photocatalysis: Transition metal ions in photocatalytic systems. Appl Catal B Environ 23:89–114
100. Cieśla P, Kocot P, Mytych P, Stasicka Z (2004) Homogeneous photocatalysis by transition metal complexes in the environment. J Mol Catal Chem 224:17–33
101. An G, Ma W, Sun Z, Liu Z, Han B, Miao S, Miao Z, Ding K (2007) Preparation of titania/carbon nanotube composites using supercritical ethanol and their photocatalytic activity for phenol degradation under visible light irradiation. Carbon 45:1795–1801
102. Wang W, Serp P, Kalck P, Faria JL (2005) Visible light photodegradation of phenol on MWNT-TiO_2 composite catalysts prepared by a modified sol-gel method. J Mol Catal Chem 235:194–199
103. Premanathan M, Karthikeyan K, Jeyasubramanian K, Manivannan G (2011) Selective toxicity of ZnO nanoparticles toward Gram-positive bacteria and cancer cells by apoptosis through lipid peroxidation. Nanomed Nanotechnol Biol Med 7:184–192
104. Sawai J, Igarashi H, Hashimoto A, Kokugan T, Shimizu M (1995) Evaluation of growth inhibitory effect of ceramics powder slurry on bacteria by conductance method. J Chem Eng Japan 28:288–293
105. Sawai J, Saito I, Kanou F, Igarashi H, Hashimoto A, Kokugan T, Shimizu M (1995) Mutagenicity test of ceramic powder which have growth inhibitory effect on bacteria. J Chem Eng Japan 28:352–354
106. Sawai J, Igarashi H, Hashimoto A, Kokugan T, Shimizu M (1996) Effect of particle size and heating temperature of ceramic powders on antibacterial activity of their slurries. J Chem Eng Japan 29:251–256
107. Sawai J, Kawada E, Kanou F, Igarashi H, Hashimoto A, Kokugan T, Shimizu M (1996) Detection of active oxygen generated from ceramic powders having antibacterial activity. J Chem Eng Japan 29:627–633
108. Sawai J, Shoji S, Igarashi H, Hashimoto A, Kokugan T, Shimizu M, Kojima H (1998) Hydrogen peroxide as an antibacterial factor in zinc oxide powder slurry. J Ferment Bioeng 86:521–522
109. Sawai J (2003) Quantitative evaluation of antibacterial activities of metallic oxide powders (ZnO, MgO and CaO) by conductimetric assay. J Microbiol Meth 54:177–182

110. Adams LK, Lyon DY, Alvarez PJJ (2006) Comparative eco-toxicity of nanoscale TiO_2, SiO_2, and ZnO water suspensions. Water Res 40:3527–3532
111. Yamamoto O, Sawai J, Sasamoto T (2000) Effect of lattice constant of zinc oxide on antibacterial characteristics. Int J Inorg Mater 2:451–454
112. Karunakaran C, Rajeswari V, Gomathisankar P (2011) Optical, electrical, photocatalytic, and bactericidal properties of microwave synthesized nanocrystalline Ag-ZnO and ZnO. Solid State Sci 13:923–928
113. Brayner R, Ferrari-Iliou R, Brivois N, Djediat S, Benedetti MF, Fiévet F (2006) Toxicological impact studies based on *Escherichia coli* bacteria in ultrafine ZnO nanoparticles colloidal medium. Nano Lett 6:866–870
114. Gajjar P, Pettee B, Britt DW, Huang W, Johnson WP, Anderson AJ (2009) Antimicrobial activities of commercial nanoparticles against an environmental soil microbe *Pseudomonas putida* KT2440. J Biol Eng 3:1183–1189
115. Huang Z, Zheng X, Yan D, Yin G, Liao X, Kang Y, Yao Y, Huang D, Hao B (2008) Toxicological effect of ZnO nanoparticles based on bacteria. Langmuir 24:4140–4144
116. Heinlaan M, Ivask A, Blinova I, Dubourguier H-C, Kahru A (2008) Toxicity of nanosized and bulk ZnO, CuO and TiO_2 to bacteria *Vibrio fischeri* and crustaceans *Daphnia magna* and *Thamnocephalus platyurus*. Chemosphere 71:1308–1316
117. Liau SY, Read DC, Pugh WJ, Furr JR, Russell AD (1997) Interaction of silver nitrate with readily identifiable groups: relationship to the antibacterialaction of silver ions. Lett Appl Microbiol 25:279–283
118. Zeiri L, Bronk BV, Shabtai Y, Eichler J, Efrima S (2004) Surface-Enhanced Raman Spectroscopy as a Tool for Probing Specific Biochemical Components in Bacteria. Appl Spectrosc 58:33–40
119. Ghandour W, Hubbard JA, Deistung J, Hughes MN, Poole RK (1988) The uptake of silver ions by *Escherichia coli* K12: toxic effects and interaction with copper ions. Appl Microbiol Biotechnol 28:559–565
120. Schreurs WJ, Rosenberg H (1982) Effect of silver ions on transport and retention of phosphate by Escherichia coli. J Bacteriol 152:7–13
121. Ohko Y, Utsumi Y, Niwa C, Tatsuma T, Kobayakawa K, Satoh Y, Kubota Y, Fujishima A (2001) Self-sterilizing and self-cleaning of silicone catheters coated with TiO_2 photocatalyst thin films: a preclinical work. J Biomed Mater Res 58:97–101
122. Agarwal A, Weis TL, Schurr MJ, Faith NG, Czuprynski CJ, McAnulty JF, Murphy CJ, Abbott NL (2010) Surfaces modified with nanometer-thick silver-impregnated polymeric films that kill bacteria but support growth of mammalian cells. Biomaterials 31:680–690
123. Feng QL, Wu J, Chen GQ, Cui FZ, Kim TN, Kim JO (2000) A mechanistic study of the antibacterial effect of silver ions on *Escherichia coli* and *Staphylococcus aureus*. J Biomed Mater Res 52:662–668
124. Sondi I, Salopek-Sondi B (2004) Silver nanoparticles as antimicrobial agent: a case study on E. coli as a model for Gram-negative bacteria. J Colloid Interface Sci 275:177–182
125. Dibrov P, Dzioba J, Gosink KK, Ha(:)se CC (2002) Chemiosmotic mechanism of antimicrobial activity of Ag^+ in *Vibrio cholerae*. Antimicrob Agents Chemother 46:2668–2670
126. Kubacka A, Cerrada ML, Serrano C, Fernandez-Garcia M, Ferrer M (2009) Plasmonic nanoparticle/polymer nanocomposites with enhanced photocatalytic antimicrobial properties. J Phys Chem C 113:9182–9190
127. Emamifar A, Kadivar M, Shahedi M, Soleimanian-Zad S (2011) Effect of nanocomposite packaging containing Ag and ZnO on inactivation of Lactobacillus plantarum in orange juice. Food Control 22:408–413
128. Manna SK, Sarkar S, Barr J, Wise K, Barrera EV, Jejelowo O, Rice-Ficht AC, Ramesh GT (2005) Single-walled carbon nanotube induces oxidative stress and activates nuclear transcription factor-kB in human keratinocytes. Nano Lett 5:1676–1684
129. Ding L, Stilwell J, Zhang T, Elboudwarej O, Jiang H, Selegue JP, Cooke PA, Gray JW, Chen FF (2005) Molecular characterization of the cytotoxic mechanism of multiwall carbon nanotubes and nano-onions on human skin fibroblast. Nano Lett 5:2448–2464

130. Shvedova AA, Kisin ER, Mercer R, Murray AR, Johnson VJ, Potapovich AI, Tyurina YY, Gorelik O, Arepalli S, Schwegler-Berry D, Hubbs AF, Antonini J, Evans DE, Ku B-K, Ramsey D, Maynard A, Kagan VE, Castranova V, Baron P (2005) Unusual inflammatory and fibrogenic pulmonary responses to single-walled carbon nanotubes in mice. Am J Physiol Lung Cell Mol Physiol 289:L698-708
131. Geslin C, Llanos J, Prieur D, Jeanthon C (2001) The manganese and iron superoxide dismutases protect Escherichia coli from heavy metal toxicity. Res Microbiol 152:901–905
132. Tang YJ, Ashcroft JM, Chen D, Min G, Kim C-H, Murkhejee B, Larabell C, Keasling JD, Chen FF (2007) Charge-associated effects of fullerene derivatives on microbial structural integrity and central metabolism. Nano Lett 7:754–760
133. Vollmer W, Blanot D, De Pedro MA (2008) Peptidoglycan structure and architecture. FEMS Microbiol Rev 32:149–167
134. Kang S, Herzberg M, Rodrigues DF, Elimelech M (2008) Antibacterial effects of carbon nanotubes: Size does matter! Langmuir 24:6409–6413
135. Davies JK, Reeves P (1975) Genetics of resistance to colicins in *Escherichia coli* K-12: cross-resistance among colicins of group A. J Bacteriol 123:102–117
136. Fognini-Lefebvre N, Lazzaroni JC, Portalier R (1987) *tolA*, *tolB*, and *excC*, three cistrons involved in the control of pleiotropic release of periplasmic proteins by *Escherichia coli* K12. Mol Gen Genet MGG 209:391–395
137. Bernadac A, Gavioli M, Lazzaroni J-C, Raina S, Lloubes R (1998) *Escherichia coli* tol-pal mutants form outer membrane vesicles. J Bacteriol 180:4872–4878
138. Murata T, Tseng W, Guina T, Miller SI, Nikaido H (2007) PhoPQ-mediated regulation produces a more robust permeability barrier in the outer membrane of *salmonella enterica serovar typhimurium*. J Bacteriol 189:7213–7222
139. Rand GM (1995) Fundamentals of Aquatic Toxicology. In: Rand GM (ed) Structure-Activity Relationships, Tayer and Francis Publisher, Washington
140. Verhaar HJM, van Leeuwen CJ, Hermens JLM (1992) Classifying environmental-pollutants 1. Structure-activity-relationships for prediction of aquatic toxicit. Chemosphere 25:471–491
141. Escher BI, Bramaz N, Eggen RIL, Richter M (2005) *In Vitro* assessment of modes of toxic action of pharmaceuticals in aquatic life. Environ Sci Technol 39:3090–3100
142. Kommireddy DS, Sriram SM, Lvov YM, Mills DK (2006) Stem cell attachment to layer-by-layer assembled TiO_2 nanoparticle thin films. Biomaterials 27:4296–4303
143. Guo D, Wu C, Jiang H, Li Q, Wang X, Chen B (2008) Synergistic cytotoxic effect of different sized ZnO nanoparticles and daunorubicin against leukemia cancer cells under UV irradiation. J Photochem Photobiol B Biol 93:119–126
144. Hanley C, Layne J, Punnoose A, Reddy K, Coombs I, Coombs A, Feris K, Wingett D (2008) Preferential killing of cancer cells and activated human T cells using ZnO nanoparticles. Nanotechnology 19:295103
145. Huang C, Aronstam RS, Chen D-R, Huang Y (2010) Oxidative stress, calcium homeostasis, and altered gene expression in human lung epithelial cells exposed to ZnO nanoparticles. Toxicol Vitro 24:45–55
146. Jin T, Sun D, Su JY, Zhang H, Sue HJ (2009) Antimicrobial efficacy of zinc oxide quantum dots against *Listeria monocytogenes*, *Salmonella Enteritidis*, and *Escherichia coli* O157:H7. J Food Sci 74:M46-M52
147. Klasen HJ (2000) Historical review of the use of silver in the treatment of burns. I. Early uses. Burns 26:117–130
148. Kristiansen S, Ifversen P, Danscher G (2008) Ultrastructural localization and chemical binding of silver ions in human organotypic skin cultures. Histochem Cell Biol 130:177–184
149. Atiyeh BS, Costagliola M, Hayek SN, Dibo SA (2007) Effect of silver on burn wound infection control and healing: review of the literature. Burns 33:139–148
150. Trop M, Novak M, Rodl S, Hellbom B, Kroell W, Goessler W (2006) Silver-coated dressing acticoat caused raised liver enzymes and argyria-like symptoms in burn patient. J Trauma 60:648–652

151. Poon VKM, Burd A (2004) *In vitro* cytotoxity of silver: implication for clinical wound care. Burns 30:140–147
152. Lee ARC, Moon HK (2003) Effect of topically applied silver sulfadiazine on fibroblast cell proliferation and biomechanical properties of the wound. Arch Pharm Res 26:855–860
153. Hussain S, Anner RM, Anner BM (1992) Cysteine protects Na, K-ATPase and isolated human lymphocytes from silver toxicity. Biochem Biophys Res Commun 189:1444–1449
154. Alt V, Bechert T, Steinrücke P, Wagener M, Seidel P, Dingeldein E, Domann E, Schnettler R (2004) An in vitro assessment of the antibacterial properties and cytotoxicity of nanoparticulate silver bone cement. Biomaterials 25:4383–4391
155. Podsiadlo P, Paternel S, Rouillard JM, Zhang Z, Lee J, Lee J-W, Gulari E, Kotov NA (2005) Layer-by-layer assembly of nacre-like nanostructured composites with antimicrobial properties. Langmuir 21:11915–11921
156. Sayes CM, Liang F, Hudson JL, Mendez J, Guo W, Beach JM, Moore VC, Doyle CD, West JL, Billups WE, Ausman KD, Colvin VL (2006) Functionalization density dependence of single-walled carbon nanotubes cytotoxicity *in vitro*. Toxicol Lett 161:135–142
157. Dumortier H, Lacotte S, Pastorin G, Marega R, Wu W, Bonifazi D, Briand J-P, Prato M, Muller S, Bianco A (2006) Functionalized carbon nanotubes are non-cytotoxic and preserve the functionality of primary immune cells. Nano Lett 6:1522–1528
158. Zhu Y, Li W, Li Q, Li Y, Li Y, Zhang X, Huang Q (2009) Effects of serum proteins on intracellular uptake and cytotoxicity of carbon nanoparticles. Carbon 47:1351–1358
159. Agarwal S, Zhou X, Ye F, He Q, Chen GCK, Soo J, Boey F, Zhang H, Chen P (2010) Interfacing live cells with nanocarbon substrates. Langmuir 26:2244–2247
160. Lovat V, Pantarotto D, Lagostena L, Cacciari B, Grandolfo M, Righi M, Spalluto G, Prato M, Ballerini L (2005) Carbon nanotube substrates boost neuronal electrical signaling. Nano Lett 5:1107–1110
161. Chang Y, Yang ST, Liu JH, Dong E, Wang Y, Cao A, Liu Y, Wang H (2011) *In vitro* toxicity evaluation of graphene oxide on A549 cells. Toxicol Lett 200:201–210
162. Chen H, Müller MB, Gilmore KJ, Wallace GG, Li D (2008) Mechanically strong, electrically conductive, and biocompatible graphene paper. Adv Mater 20:3557–3561
163. Stewart PS, Costerton WJ (2001) Antibiotic resistance of bacteria in biofilms. Lancet 358:135–138
164. Adolfsson-Erici M, Pettersson M, Parkkonen J, Sturve J (2002) Triclosan, a commonly used bactericide found in human milk and in the aquatic environment in Sweden. Chemosphere 46:1485–1489
165. Sekiguchi Y, Yao Y, Ohko Y, Tanaka K, Ishido T, Fujishima A, Kubota Y (2007) Self-sterilizing catheters with titanium dioxide photocatalyst thin films for clean intermittent catheterization: basis and study of clinical use. Int J Urol 14:426–430